creative commons
COMMONS DEED

저작자표시-비영리-변경금지 2.0 대한민국

이용자는 아래의 조건을 따르는 경우에 한하여 자유롭게

- 이 저작물을 복제, 배포, 전송, 전시, 공연 및 방송할 수 있습니다.

다음과 같은 조건을 따라야 합니다:

저작자표시. 귀하는 원저작자를 표시하여야 합니다.

비영리. 귀하는 이 저작물을 영리 목적으로 이용할 수 없습니다.

변경금지. 귀하는 이 저작물을 개작, 변형 또는 가공할 수 없습니다.

- 귀하는, 이 저작물의 재이용이나 배포의 경우, 이 저작물에 적용된 이용허락조건을 명확하게 나타내어야 합니다.
- 저작권자로부터 별도의 허가를 받으면 이러한 조건들은 적용되지 않습니다.

저작권법에 따른 이용자의 권리는 위의 내용에 의하여 영향을 받지 않습니다.

이것은 이용허락규약(Legal Code)을 이해하기 쉽게 요약한 것입니다.

Disclaimer

dCollection

공학박사 학위논문

Stress and Strain Analysis of Rotating Annular Disks Obeying a Pressure-Dependent Yield Criterion

압력 의존적 항복조건을 만족하는 회전 환상 원판의 응력과 변형율 분석

2017년 2월

서울대학교 대학원

재료공학부

정 원 철

Stress and Strain Analysis of Rotating Annular Disks Obeying a Pressure-Dependent Yield Criterion

압력 의존적 항복조건을 만족하는 회전 환상 원판의 응력과 변형율 분석

지도 교수 정 관 수

이 논문을 공학박사 학위논문으로 제출함
2016년 12월

서울대학교 대학원
재료공학부
정 원 철

정원철의 박사 학위논문을 인준함
2016년 12월

위 원 장 유 웅 열 (인)

부위원장 정 관 수 (인)

위 원 한 흥 남 (인)

위 원 이 명 규 (인)

위 원 김 대 용 (인)

Abstract

Stress and Strain Analysis of Rotating Annular Disks Obeying a Pressure-Dependent Yield Criterion

Woncheol Jeong
Department of Materials Science and Engineering
The Graduate School
Seoul National University

The Drucker - Prager yield criterion is used in conjunction with its associated flow rule to find the elastic/plastic stress and strain distributions within the rotating annular disks under plane stress conditions. The main distinguished feature of the model, as compared to typical models used for analysis of rotating disks, is that the material is plastically compressible. Also, in contrast to many models used for analysis of rotating disks, the constitutive equations involve strain rates rather than strains. However, using an approach proposed elsewhere the solution for strain rates is reduced to one non-linear ordinary differential equation and two linear ordinary differential equations. These equations can be solved one by one, which significantly simplifies the numerical treatment and increases the accuracy of numerical solution.

The strain solution requires a numerical technique to evaluate ordinary integrals. An example is presented to illustrate the general solution. The primary objective of this paper is to examine the effect of the parameter that controls the deviation of the Drucker-Prager yield criterion from the von Mises yield criterion and the geometric parameter that controls the profile of hyperbolic discs on the stress distribution at loading and the residual stress distribution.

Keywords: rotating annular disc, plastic yielding, Drucker-Prager yield criterion

Student Number: 2012-30919

Contents

List of Figures

Chapter 1. Introduction

The Tresca yield criterion in conjunction with its associated flow rule has long been associated with the solution to the stresses and strains in thin rotating disks under plane stress conditions (Guven, 1992, 1998; Orchan and Eraslan, 2002; Eraslan and Orcan, 2002A, 2002B; Eraslan, 2002, 2003). A mathematical advantage of this model is that the equations for strain rates can be integrated with respect to the time (or any time-like parameter) giving the corresponding equations for strains. Therefore, the original flow theory of plasticity reduces to the corresponding deformation theory of plasticity. A number of solutions for the deformation theory of plasticity used in conjunction with the von Mises yield criterion are also available (Eraslan, 2003; You *et al*., 2000; Hojjati and Hassani, 2008). The stress distributions in rotating disks from von Mises and Tresca yield criteria have been compared in Rees (1999). It has been shown that the choice of the yield criterion may affect the final result. It is generally accepted that the deformation theory of plasticity is valid only when dealing with proportional loadings. On the other hand, it is known that the strain path is in general not proportional in thin disks (Piruvmov *et al*., 2013). It is therefore of interest to find the distribution of stresses and strains in thin rotating disks using the flow theory of plasticity. Finite difference solutions for such material models have been given in Alexandrova *et al*. (2004) and Alexandrova (2012). Recently, an approach to find a semi-analytic solution for the von Mises yield criterion and its associated flow rule has been proposed in Lomakin *et al*. (2016). An advantage of this approach is that the original boundary value problems in two independent variables is reduced to solving

several ordinary differential equations (these equations can be solved one by one) and to evaluating ordinary integrals. In the present paper, the approach developed in Lomakin *et al*. (2016) is extended to the yield criterion proposed in Drucker and Prager (1952). The flow rule associated with this yield criterion predicts that the material is plastically compressible. This material model is appropriate for several metallic materials (Wilson, 2002; Liu, 2006). The corresponding stress solution for a hyperbolic disk has been given in Jeong and Chung (2016). The solution of the disk of constant thickness can be found as a special case.

Rotating discs are widely used in mechanical engineering and a great number of solutions for elastic/plastic disc are available in the literature. A review of solutions for discs of constant thickness obeying the Tresca and von Mises yield criteria has been provided in Rees (1999). But, discs of variable thickness are advantageous for many applications. There are a great number of solutions for such discs as well; however, most of analytic solutions are for the Tresca yield criterion and Hencky's deformation theory of plasticity. The latter is usually based on the von Mises yield criterion.

Many metallic materials reveal pressure-dependence of plastic yielding. Bend tests under superimposed hydrostatic pressure on a low carbon steel containing globular sulfide inclusions show that formability is improved by increasing pressure due to a pressure-induced transition in fracture mechanism (Spitzig *et al.*, 1976). The consequences for maraging and HY-80 steels show a strong, but not perfect, correlation between pressure dependence, yield stress, and volume expansion; but, the volume expansion is strongly thought to be the primary result from the production of new dislocations: this volume change is very small and does not seem to be essential to the pressure dependence. Most of the pressure dependence is accountable for the discrepancy with the normality flow rule and may has an effect on dislocation motion. Therefore, appropriate plasticity model would be suggested to be one in which the

octahedral shear yield stress has a linear dependence on the mean pressure, but the volume change is negligible in violation of the normality flow rule (Kao *et al.*, 1990). New experiments and nonlinear finite element analyses of 2024-T351 aluminum notched round bars have measured the quantification of effect of hydrostatic tensile stresses on yielding (Wilson, 2002). On the basis of a new simplified structural model of three-dimensional isotropic reticulated foamed porous metals, a practical analytical model is developed for these materials under biaxial loading. From this new mechanical model, an effective correlation between biaxial nominal stresses and porosity at the commencement of failure is derived for metallic foams under biaxial tension (Liu, 2006).

It has been demonstrated in Alexandrov *et al*. (2011) and Pirumov *et al*. (2013) that this material property may have a significant effect on the distribution of stresses in thin discs. However, available solutions for rotating discs do not account for pressure-dependence of plastic yielding. The present paper provides such a solution for an annular disc assuming that the yield criterion proposed in Drucker and Prager (1952) is valid.

Chapter 2. Disk of constant thickness

2.1 Statement of the problem

Consider a thin annular disk of outer radius b_0 and inner radius a_0 rotating with an angular velocity ω about its axis. The thickness of the dick is constant. Strains are supposed to be infinitesimal. The disk has no stress at $\omega = 0$. It is natural to introduce a cylindrical coordinate system (r, θ, z) with the *z*-axis coinciding with the axis of symmetry of the disk.

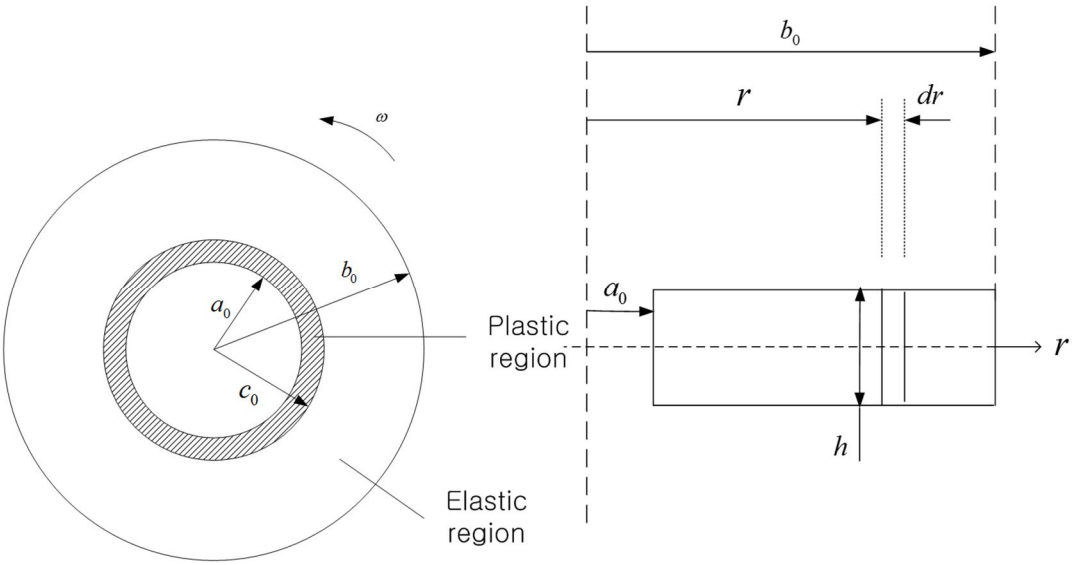

Figure 1 Disk configuration

Let σ_r, σ_θ and σ_z be the normal stresses relative to this coordinate system. These stresses are the principal stresses. The boundary value problem is axisymmetric, and its solution is independent of s. The circumferential displacement vanishes everywhere. The state of stress in the rotating disk is two-dimensional ($\sigma_z = 0$). The angular velocity ω slowly increases from zero to some prescribed value. Therefore, the component of the acceleration vector in the circumferential direction is neglected. The boundary conditions are

$$\sigma_r = 0 \tag{2.1.1}$$

for $r = a_0$ and $r = b_0$. In general, the disk consists of two regions, elastic and plastic. The elastic strains are related by Hooke's law to the stresses. In the case under consideration this law in the cylindrical coordinate system reads

$$\varepsilon_r^e = \frac{\sigma_r - \nu\sigma_\theta}{E}, \quad \varepsilon_\theta^e = \frac{\sigma_\theta - \nu\sigma_r}{E}, \quad \varepsilon_z^e = -\frac{\nu\left(\sigma_r + \sigma_\theta\right)}{E}. \tag{2.1.2}$$

Here ν is Poisson's ratio and *E* is Young's modulus. The superscript *e* denotes the elastic part of the strain and will denote the elastic part of the strain rate as well. In the elastic region, the whole strain is elastic. The superscript *e* is employed in equation (2.1.2) as the same equations are satisfied by the elastic part of the strain in the plastic region. The superscript can be dropped in the elastic region. It is assumed that the yield

criterion proposed in Drucker and Prager (1952) and its associated flow rule are valid in the plastic region. This yield criterion is written in plane stress as

$$\left(1-\frac{\alpha^2}{9}\right)\left(\sigma_r^2+\sigma_\theta^2\right)-\left(1+\frac{2\alpha^2}{9}\right)\sigma_r\sigma_\theta+\frac{2\alpha}{3}\sigma_0\left(\sigma_r+\sigma_\theta\right)=\sigma_0^2. \tag{2.1.3}$$

The constitutive parameters, α and σ_0, are constant. The yield criterion (2.1.3) reduces to the von Mises yield criterion at $\alpha=0$. In this case, s is the tensile yield stress. Let $\dot{\varepsilon}_r^p$, $\dot{\varepsilon}_\theta^p$ and $\dot{\varepsilon}_z^p$ be the plastic strain rates. The associated flow rule under plane stress conditions can be written as Alexanddrov (2015).

$$\begin{aligned}
\dot{\varepsilon}_r^p &= \lambda\left[6\alpha\sigma_0+2\left(9-\alpha^2\right)\sigma_r-\left(2\alpha^2+9\right)\sigma_\theta\right],\\
\dot{\varepsilon}_\theta^p &= \lambda\left[6\alpha\sigma_0+2\left(9-\alpha^2\right)\sigma_\theta-\left(2\alpha^2+9\right)\sigma_r\right],\\
\dot{\varepsilon}_z^p &= \lambda\left[6\alpha\sigma_0-\left(9+2\alpha^2\right)\left(\sigma_r+\sigma_\theta\right)\right].
\end{aligned} \tag{2.1.4}$$

where λ is a non-negative multiplier. The superimposed dot denotes the time derivative at fixed *r* and the superscript *p* denotes the plastic part of the strain rate and will denote the plastic part of the strain. It is seen from (2.1.4) that $\dot{\varepsilon}_r^p+\dot{\varepsilon}_\theta^p+\dot{\varepsilon}_z^p\neq 0$. Therefore, the material is plastically compressible. The total strains and strain rates in the plastic region are

$$\begin{aligned}
&\varepsilon_r = \varepsilon_r^e + \varepsilon_r^p, \quad \varepsilon_\theta = \varepsilon_\theta^e + \varepsilon_\theta^p, \quad \varepsilon_z = \varepsilon_z^e + \varepsilon_z^p, \\
&\dot{\varepsilon}_r = \dot{\varepsilon}_r^e + \dot{\varepsilon}_r^p, \quad \dot{\varepsilon}_\theta = \dot{\varepsilon}_\theta^e + \dot{\varepsilon}_\theta^p, \quad \dot{\varepsilon}_z = \dot{\varepsilon}_z^e + \dot{\varepsilon}_z^p.
\end{aligned} \tag{2.1.5}$$

The constitutive equations should be supplemented with the equilibrium equation of the form

$$\frac{\partial \sigma_r}{\partial r} + \frac{\sigma_r - \sigma_\theta}{r} = -\varsigma \omega^2 r\,. \tag{2.1.6}$$

Here ς is the density of the material.

It is convenient to introduce the following dimensionless quantities

$$\rho = \frac{r}{b_0}, \quad \Omega = \frac{\sqrt{3}\varsigma \omega^2 b_0^2}{\sigma_0}, \quad a = \frac{a_0}{b_0}, \quad k = \frac{\sigma_0}{E}. \tag{2.1.7}$$

The material model adopted is rate-independent. Therefore, the time derivative can be replaced with the derivative with respect to any monotonically increasing parameter. In particular, it is convenient to introduce the following quantities

$$\begin{aligned}
&\xi_r = \frac{\partial \varepsilon_r}{\partial \Omega}, \quad \xi_\theta = \frac{\partial \varepsilon_\theta}{\partial \Omega}, \quad \xi_z = \frac{\partial \varepsilon_z}{\partial \Omega}, \\
&\xi_r^e = \frac{\partial \varepsilon_r^e}{\partial \Omega}, \quad \xi_\theta^e = \frac{\partial \varepsilon_\theta^e}{\partial \Omega}, \quad \xi_z^e = \frac{\partial \varepsilon_z^e}{\partial \Omega}, \\
&\xi_r^p = \frac{\partial \varepsilon_r^p}{\partial \Omega}, \quad \xi_\theta^p = \frac{\partial \varepsilon_\theta^p}{\partial \Omega}, \quad \xi_z^p = \frac{\partial \varepsilon_z^p}{\partial \Omega}.
\end{aligned} \tag{2.1.8}$$

The equation of strain rate compatibility is equivalent to

$$\rho \frac{\partial \xi_\theta}{\partial \rho} = \xi_r - \xi_\theta . \tag{2.1.9}$$

Using (2.1.7) equation (2.1.6) can be transformed to

$$\frac{\partial \sigma_r}{\sigma_0 \partial \rho} + \frac{\sigma_r - \sigma_\theta}{\sigma_0 \rho} = -\frac{\Omega \rho}{\sqrt{3}} . \tag{2.1.10}$$

2.2 Solution

2.2.1 Purely elastic solution

The purely elastic solution of the boundary value problem under consideration is well known (see, for example, Timoshenko and Goodier, 1970). Using (2.1.7) the solution satisfying the boundary condition (2.1.1) at $\rho = 1$ can be written as

$$
\begin{aligned}
&\frac{\sigma_r}{\sigma_0} = A\left(\frac{1}{\rho^2}-1\right)+\frac{\Omega(3+\nu)}{8\sqrt{3}}\left(1-\rho^2\right),\\
&\frac{\sigma_\theta}{\sigma_0} = -A\left(\frac{1}{\rho^2}+1\right)+\frac{\Omega(1+3\nu)}{8\sqrt{3}}\left(\frac{3+\nu}{1+3\nu}-\rho^2\right),\\
&\frac{\varepsilon_r}{k} = \frac{24A\left[1+\nu-(1-\nu)\rho^2\right]+\sqrt{3}\Omega(1-\nu)\left[3+\nu-3(1+\nu)\rho^2\right]\rho^2}{24\rho^2},\\
&\frac{\varepsilon_\theta}{k} = \frac{-24A\left[1+\nu+(1-\nu)\rho^2\right]+\sqrt{3}\Omega(1-\nu)\left[3+\nu-(1+\nu)\rho^2\right]\rho^2}{24\rho^2},\\
&\frac{\varepsilon_z}{k} = \frac{\nu}{12}\left\{24A-\sqrt{3}\Omega\left[3+\nu-2(1+\nu)\rho^2\right]\right\}.
\end{aligned}
\tag{2.2.1}
$$

Here A is a constant of integration. Using the boundary condition (2.1.1) at $\rho = a$ this constant is determined as

$$
A = -\frac{\Omega(3+\nu)a^2}{8\sqrt{3}}. \tag{2.2.2}
$$

Substituting (2.2.2) into (2.2.1) supplies the distribution of the stresses and strains in the purely elastic disk. In particular,

$$
\frac{\sigma_r}{\sigma_0} = 0, \quad \frac{\sigma_\theta}{\sigma_0} = \frac{\Omega\left[3+\nu+a^2(1-\nu)\right]}{4\sqrt{3}} \tag{2.2.3}
$$

at $\rho = a$. Substituting (2.2.3) into the yield criterion (2.1.3) shows that

$$\Omega_e = \frac{12\sqrt{3}}{(3+\alpha)\left[3+\nu+a^2(1-\nu)\right]} \tag{2.2.4}$$

where Ω_e is the value of Ω at which the plastic region starts to develop from the inner radius of the disk. In what follows, it is assumed that $\Omega > \Omega_e$.

The solution (2.2.1) is also valid in the elastic region of the elastic/plastic disk. However, A is not given by (2.2.2).

2.2.2 Elastic/Plastic stress solution

The elastic/plastic stress solution is available in Jeong and Chung (2016). For completeness, this solution is outlined below. The yield criterion (2.1.3) is satisfied by the following substitution (Alexandrov *et al*., 2014)

$$\begin{aligned}
\frac{\sigma_r}{\sigma_0} &= 3\beta_0 + \frac{\beta_1}{2}\left(1+3\sqrt{3}\beta_1\right)\sin\psi - \frac{\sqrt{3}}{2}\beta_1\left(1-\sqrt{3}\beta_1\right)\cos\psi, \\
\frac{\sigma_\theta}{\sigma_0} &= 3\beta_0 - \frac{\beta_1}{2}\left(1-3\sqrt{3}\beta_1\right)\sin\psi + \frac{\sqrt{3}}{2}\beta_1\left(1+\sqrt{3}\beta_1\right)\cos\psi, \\
\beta_0 &= \frac{2\alpha}{4\alpha^2-9}, \quad \beta_1 = \frac{\sqrt{3}}{\sqrt{9-4\alpha^2}}
\end{aligned} \tag{2.2.5}$$

where ψ is a new function of ρ and Ω. Substituting (2.2.5) into (2.1.10) gives

$$\left[\left(\sqrt{3}-3\beta_1\right)\sin\psi+\left(1+3\sqrt{3}\beta_1\right)\cos\psi\right]\frac{\partial\psi}{\partial\rho}+\frac{2\left(\sin\psi-\sqrt{3}\cos\psi\right)}{\rho}=-\frac{2\Omega\rho}{\sqrt{3}\beta_1}. \quad (2.2.6)$$

Let ψ_a be the value of ψ at $\rho=a$. It follows from the boundary condition (2.1.1) at $\rho=a$ and (2.2.5) that the value of ψ_a is determined from the equations

$$3\beta_0+\frac{\beta_1}{2}\left(1+3\sqrt{3}\beta_1\right)\sin\psi_a-\frac{\sqrt{3}}{2}\beta_1\left(1-\sqrt{3}\beta_1\right)\cos\psi_a=0,$$
$$3\beta_0-\frac{\beta_1}{2}\left(1-3\sqrt{3}\beta_1\right)\sin\psi_a+\frac{\sqrt{3}}{2}\beta_1\left(1+\sqrt{3}\beta_1\right)\cos\psi_a>0.$$

These equations should be solved numerically. Then, the boundary condition to equation (2.2.6) is

$$\psi=\psi_a \quad (2.2.7)$$

for $\rho=a$. Let ρ_c be the dimensionless radius of the elastic/plastic boundary and ψ_c be the value of ψ at $\rho=\rho_c$. The radial and circumferential stresses should be

continuous across the elastic/plastic boundary. Therefore, it follows from (2.2.1) and (2.2.5) that

$$A\left(\frac{1}{\rho_c^2}-1\right)+\frac{\Omega(3+\nu)}{8\sqrt{3}}\left(1-\rho_c^2\right)=3\beta_0+\frac{\beta_1}{2}\left(1+3\sqrt{3}\beta_1\right)\sin\psi_c-\frac{\sqrt{3}}{2}\beta_1\left(1-\sqrt{3}\beta_1\right)\cos\psi_c, \tag{2.2.8}$$
$$-A\left(\frac{1}{\rho_c^2}+1\right)+\frac{\Omega(1+3\nu)}{8\sqrt{3}}\left(\frac{3+\nu}{1+3\nu}-\rho_c^2\right)=3\beta_0-\frac{\beta_1}{2}\left(1-3\sqrt{3}\beta_1\right)\sin\psi_c+\frac{\sqrt{3}}{2}\beta_1\left(1+\sqrt{3}\beta_1\right)\cos\psi_c.$$

Eliminating A between these equations results in

$$6\beta_0+\beta_1\left[\left(3\beta_1-\sqrt{3}\rho_c^2\right)\cos\psi_c+\left(3\sqrt{3}\beta_1+\rho_c^2\right)\sin\psi_c\right]-\frac{\Omega}{4\sqrt{3}}\left(1-\rho_c^2\right)\left[3+\nu+(1-\nu)\rho_c^2\right]=0. \tag{2.2.9}$$

This equation and the solution of equation (2.2.6) constitute the set of equations to find ρ_c and ψ_c at a given value of Ω. Then, A can be determined from any of equations (2.2.8). The distribution of the stresses in the elastic region, $\rho_c \le \rho \le 1$, follows from (2.2.1). The distribution of the stresses in the plastic region, $a \le \rho \le \rho_c$, can be found from (2.2.5) and the solution of equation (2.2.6) in parametric form with ψ being the parameter. The entire disk becomes plastic when $\rho_c = 1$. The corresponding value of Ω is denoted by Ω_p. This value can be calculated numerically since the dependence of ρ_c on Ω has been already found from (2.2.9) and the solution of equation (2.2.6).

2.2.3 Elastic/Plastic strain solution

The strain solution in the elastic region follows from (2.2.1) where A should be expressed in terms of Ω by means of the solution of equations (2.2.8) and (2.2.9). Eliminating λ in (2.1.4), replacing the time derivative with the derivative with respect to Ω and using (2.1.8) lead to

$$\xi_r^p = \xi_\theta^p \left[\frac{6\alpha\sigma_0 + 2\left(9-\alpha^2\right)\sigma_r - \left(2\alpha^2+9\right)\sigma_\theta}{6\alpha\sigma_0 + 2\left(9-\alpha^2\right)\sigma_\theta - \left(2\alpha^2+9\right)\sigma_r} \right], \quad \xi_z^p = \xi_\theta^p \left[\frac{6\alpha\sigma_0 - \left(9+2\alpha^2\right)\left(\sigma_r+\sigma_\theta\right)}{6\alpha\sigma_0 + 2\left(9-\alpha^2\right)\sigma_\theta - \left(2\alpha^2+9\right)\sigma_r} \right].$$

Eliminating the stresses in these equations by means of (2.2.5) yields

$$\begin{aligned} \xi_r^p &= \xi_\theta^p \left[\frac{\beta_1\left(\sqrt{3}-\beta_1\right)\cos\psi - \beta_1\left(1+\sqrt{3}\beta_1\right)\sin\psi + 2\beta_0}{\beta_1\left(1-\sqrt{3}\beta_1\right)\sin\psi - \beta_1\left(\sqrt{3}+\beta_1\right)\cos\psi + 2\beta_0} \right], \\ \xi_z^p &= 2\xi_\theta^p \left[\frac{\beta_1^2\left(\cos\psi + \sqrt{3}\sin\psi\right) - 2\beta_0}{\beta_1\left(1-\sqrt{3}\beta_1\right)\sin\psi - \beta_1\left(\sqrt{3}+\beta_1\right)\cos\psi + 2\beta_0} \right]. \end{aligned} \tag{2.2.10}$$

The elastic strains in the plastic region are found from (2.1.2), (2.1.7) and (2.2.5) as

$$\begin{aligned} \frac{\varepsilon_r^e}{k} &= 3\beta_0\left(1-\nu\right) + \frac{\sqrt{3}\beta_1}{2}\left[\sqrt{3}\beta_1\left(1-\nu\right) - 1 - \nu\right]\cos\psi + \frac{\beta_1}{2}\left[3\sqrt{3}\beta_1\left(1-\nu\right) + 1 + \nu\right]\sin\psi, \\ \frac{\varepsilon_\theta^e}{k} &= 3\beta_0\left(1-\nu\right) + \frac{\sqrt{3}\beta_1}{2}\left[\sqrt{3}\beta_1\left(1-\nu\right) + 1 + \nu\right]\cos\psi + \frac{\beta_1}{2}\left[3\sqrt{3}\beta_1\left(1-\nu\right) - 1 - \nu\right]\sin\psi, \\ \frac{\varepsilon_z^e}{k} &= -3\nu\left[2\beta_0 + \beta_1^2\left(\cos\psi + \sqrt{3}\sin\psi\right)\right]. \end{aligned} \tag{2.2.11}$$

Then,

$$\begin{aligned}
\frac{\xi_r^e}{k} &= \frac{\beta_1}{2}\left\{\left[3\sqrt{3}\beta_1(1-\nu)+1+\nu\right]\cos\psi-\sqrt{3}\left[\sqrt{3}\beta_1(1-\nu)-1-\nu\right]\sin\psi\right\}\frac{\partial\psi}{\partial\Omega},\\
\frac{\xi_\theta^e}{k} &= \frac{\beta_1}{2}\left\{\left[3\sqrt{3}\beta_1(1-\nu)-1-\nu\right]\cos\psi-\sqrt{3}\left[\sqrt{3}\beta_1(1-\nu)+1+\nu\right]\sin\psi\right\}\frac{\partial\psi}{\partial\Omega},\\
\frac{\xi_z^e}{k} &= 3\nu\beta_1^2\left(\sin\psi-\sqrt{3}\cos\psi\right)\frac{\partial\psi}{\partial\Omega}.
\end{aligned} \qquad (2.2.12)$$

Taking into account (2.1.5) equation (2.1.9) can be rewritten as

$$\rho\frac{\partial\xi_\theta}{\partial\rho}=\xi_r^p+\xi_r^e-\xi_\theta^p-\xi_\theta^e .$$

Using (2.2.10) this equation can be transformed to

$$\rho\frac{\partial\xi_\theta}{\partial\rho}=\frac{4\beta_1\xi_\theta^p\cos\left(\psi+\pi/6\right)}{\left[2\beta_0+\beta_1\left(1-\sqrt{3}\beta_1\right)\sin\psi-\beta_1\left(\sqrt{3}+\beta_1\right)\cos\psi\right]}+\xi_r^e-\xi_\theta^e .$$

This equation and (2.1.5) combine to give the following equation for ξ_θ

$$\begin{aligned}
&\rho\frac{\partial\xi_\theta}{\partial\rho}-\frac{4\beta_1\xi_\theta\cos\left(\psi+\pi/6\right)}{\left[2\beta_0+\beta_1\left(1-\sqrt{3}\beta_1\right)\sin\psi-\beta_1\left(\sqrt{3}+\beta_1\right)\cos\psi\right]}+\\
&\frac{\left[2\beta_0-\beta_1\left(1+\sqrt{3}\beta_1\right)\sin\psi+\beta_1\left(\sqrt{3}-\beta_1\right)\cos\psi\right]}{\left[2\beta_0+\beta_1\left(1-\sqrt{3}\beta_1\right)\sin\psi-\beta_1\left(\sqrt{3}+\beta_1\right)\cos\psi\right]}\xi_\theta^e-\xi_r^e=0
\end{aligned} \qquad (2.2.13)$$

Using (2.2.12) it is possible to eliminate ξ_r^e and ξ_θ^e in (2.2.13). It is therefore

evident that (2.2.13) is a linear ordinary differential equation. However, to solve this equation it is necessary to determine the derivative $\partial\psi/\partial\Omega$ involved in (2.2.12) in terms of ψ or/and ρ. To this end, equation (2.2.6) is differentiated with respect to Ω. As a result,

$$\begin{aligned}&\left[\left(\sqrt{3}-3\beta_1\right)\sin\psi+\left(1+3\sqrt{3}\beta_1\right)\cos\psi\right]\frac{\partial\chi}{\partial\rho}+\\&\left\{\frac{2\left(\cos\psi+\sqrt{3}\sin\psi\right)}{\rho}+\left[\left(\sqrt{3}-3\beta_1\right)\cos\psi-\left(1+3\sqrt{3}\beta_1\right)\sin\psi\right]\frac{\partial\psi}{\partial\rho}\right\}\chi+\frac{2\rho}{\sqrt{3}\beta_1}=0\end{aligned}\tag{2.2.14}$$

where $\chi=\partial\psi/\partial\Omega$. The derivative $\partial\psi/\partial\rho$ in equation (2.2.14) can be eliminated by means of equation (2.2.6). Then, equation (2.2.14) becomes

$$\begin{aligned}&\left[\left(\sqrt{3}-3\beta_1\right)\sin\psi+\left(1+3\sqrt{3}\beta_1\right)\cos\psi\right]\frac{\partial\chi}{\partial\rho}+\\&\left\{\begin{array}{l}\dfrac{2\left(\cos\psi+\sqrt{3}\sin\psi\right)}{\rho}+\\\dfrac{2\left[\sqrt{3}\beta_1\left(\sqrt{3}\cos\psi-\sin\psi\right)-\Omega\rho^2\right]\left[\left(\sqrt{3}-3\beta_1\right)\cos\psi-\left(1+3\sqrt{3}\beta_1\right)\sin\psi\right]}{\sqrt{3}\beta_1\rho\left[\left(\sqrt{3}-3\beta_1\right)\sin\psi+\left(1+3\sqrt{3}\beta_1\right)\cos\psi\right]}\end{array}\right\}\chi+\frac{2\rho}{\sqrt{3}\beta_1}=0.\end{aligned}\tag{2.2.15}$$

It is seen from the boundary condition (2.2.7) that $\partial\psi/\partial\Omega=0$ at $\rho=a$. Therefore, the boundary condition to equation (2.2.15) is

$$\chi=0\tag{2.2.16}$$

for $\rho=a$. It is evident that (2.2.15) is a linear ordinary differential equation for χ. This equation should be solved numerically since its coefficients are numerical functions of ρ and are determined from the solution of equation (2.2.6). Once equation (2.2.15) has been solved for χ, it is possible to express ξ_r^e and ξ_θ^e

involved in (2.2.13) as functions of ψ and ρ by means of (2.2.12). Since ψ is a known function of ρ due to the solution of equation (2.2.6), the coefficients of equation (2.2.13) are functions of ρ and this ordinary differential equation can be solved numerically with no difficulty.

The boundary condition to equation (2.2.13) is derived from the condition that $\left[\xi_\theta\right]=0$ at $\rho=\rho_c$. Here $\left[...\right]$ denotes the amount of jump in the quantity enclosed in the brackets. The value of ξ_θ on the elastic side of the elastic/plastic boundary is determined from (2.2.1) as

$$\frac{\xi_c}{k}=\frac{\sqrt{3}(1-\nu)\left[3+\nu-(1+\nu)\rho_c^2\right]}{24}-\frac{\left[1+\nu+(1-\nu)\rho_c^2\right]}{\rho_c^2}\frac{dA}{d\Omega}. \tag{2.2.17}$$

Therefore, the boundary condition to equation (2.2.13) is

$$\xi_\theta=\xi_c \tag{2.2.18}$$

for $\rho=\rho_c$. Once equation (2.2.13) has been be solved numerically, the total circumferential strain in the plastic region is found by integration of ξ_θ with respect to Ω at a given value of $\rho=\rho_t$. Let Ω_f be the value of Ω at which the radial distribution of the circumferential strain should be calculated. The value of ρ_c corresponding to $\Omega=\Omega_f$ is denoted by ρ_f. It is evident that $a\le\rho_t<\rho_f$. The

value of Ω at $\rho_c = \rho_t$ is denoted by Ω_t. Then,

$$\varepsilon_\theta = \int_{\Omega_c}^{\Omega_f} \xi_\theta d\Omega + E_\theta^t. \tag{2.2.19}$$

Here E_θ^t is the circumferential strain on the elastic side of the elastic/plastic boundary at $\rho_c = \rho_t$.

This strain is found from (2.2.1) as

$$\frac{E_\theta^t}{k} = \frac{-24A_t\left[1+\nu+(1-\nu)\rho_t^2\right]+\sqrt{3}\Omega_t(1-\nu)\left[3+\nu-(1+\nu)\rho_t^2\right]\rho_t^2}{24\rho_t^2}. \tag{2.2.20}$$

Here A_t is the value of A at $\rho_c = \rho_t$. This value is determined from (2.2.8) and (2.2.9). It follows from equations (2.1.5) and (2.2.12) that

$$\xi_\theta^p = \xi_\theta - \frac{k\beta_1}{2}\left\{\left[3\sqrt{3}\beta_1(1-\nu)-1-\nu\right]\cos\psi - \sqrt{3}\left[\sqrt{3}\beta_1(1-\nu)+1+\nu\right]\sin\psi\right\}\chi. \tag{2.2.21}$$

Substituting equation (2.2.21) into equation (2.2.10) yields

$$\frac{\xi_r^p}{k}=\left\langle \frac{\xi_\theta}{k}-\frac{\beta_1}{2}\left\{\left[3\sqrt{3}\beta_1(1-\nu)-1-\nu\right]\cos\psi-\sqrt{3}\left[\sqrt{3}\beta_1(1-\nu)+1+\nu\right]\sin\psi\right\}\chi\right\rangle\times$$
$$\left[\frac{\beta_1\left(\sqrt{3}-\beta_1\right)\cos\psi-\beta_1\left(1+\sqrt{3}\beta_1\right)\sin\psi+2\beta_0}{\beta_1\left(1-\sqrt{3}\beta_1\right)\sin\psi-\beta_1\left(\sqrt{3}+\beta_1\right)\cos\psi+2\beta_0}\right], \tag{2.2.22}$$
$$\frac{\xi_z^p}{k}=2\left\langle \frac{\xi_\theta}{k}-\frac{\beta_1}{2}\left\{\left[3\sqrt{3}\beta_1(1-\nu)-1-\nu\right]\cos\psi-\sqrt{3}\left[\sqrt{3}\beta_1(1-\nu)+1+\nu\right]\sin\psi\right\}\chi\right\rangle\times$$
$$\left[\frac{\beta_1^2\left(\cos\psi+\sqrt{3}\sin\psi\right)-2\beta_0}{\beta_1\left(1-\sqrt{3}\beta_1\right)\sin\psi-\beta_1\left(\sqrt{3}+\beta_1\right)\cos\psi+2\beta_0}\right].$$

Then,

$$\frac{\varepsilon_r^p}{k}=\int_{\Omega_t}^{\Omega_f}\frac{\xi_r^p}{k}d\Omega,\quad \frac{\varepsilon_z^p}{k}=\int_{\Omega_t}^{\Omega_f}\frac{\xi_z^p}{k}d\Omega. \tag{2.2.23}$$

Here the integrands are known functions of Ω due to the solution to equations (2.2.6), (2.2.13) and (2.2.15) and equation (2.2.22). Therefore, the integrals involved in (2.2.23) can be evaluated numerically. The total radial and axial strains in the plastic zone are found by summing the plastic parts given by (2.2.23) and the elastic parts given by (2.2.11).

2.3 Illustrative example

Equations (2.2.6), (2.2.14) and (2.2.13) have been solved numerically in the range $\Omega_e \le \Omega \le \Omega_p$ at $a = 0.3$ and $a = 0.5$ for $\nu = 0.3$ and several typical values of α. The variation of the radial and circumferential stresses with ρ in an $a = 0.3$ disk at the value of the angular velocity corresponding to $\rho_c = 0.6$ is depicted in Figures 2 and 3, respectively. The associated strain distributions have been found from equations (2.1.2), (2.1.5), (2.2.19), and (2.2.23) at the same values of Ω. The distributions of the total strains are shown in Figure 4 (radial strain), Figure 5 (circumferential strain) and Figure 6 (axial strain). The variation of the plastic strains with ρ is depicted in Figure 7 (radial strain), Figure 8 (circumferential strain) and Figure 9 (axial strain). The variation of the radial and circumferential stresses with ρ in an $a = 0.5$ disk at the value of the angular velocity corresponding to $\rho_c = 0.75$ is depicted in Figures 10 and 11, respectively. The associated strain distributions have been found from equations (2.1.2), (2.1.5), (2.2.19), and (2.2.23) at the same values of Ω. The distributions of the total strains are shown in Figure 12 (radial strain), Figure 13 (circumferential strain) and Figure 14 (axial strain). The variation of the plastic strains with ρ is depicted in Figure 15 (radial strain), Figure 16 (circumferential strain) and Figure 17 (axial strain).

It is seen from Figs. 3 and 11 that the value of α has a significant effect of the distribution of the circumferential stress. The effect of $\alpha -$ value of the total strains is pronounced for the axial strain in the vicinity of the inner radius (Figs. 6 and 14). The effect of this value on the distribution of the plastic strain is in general more significant than on the total strains (Figs. 4 – 9 and 12 – 17).

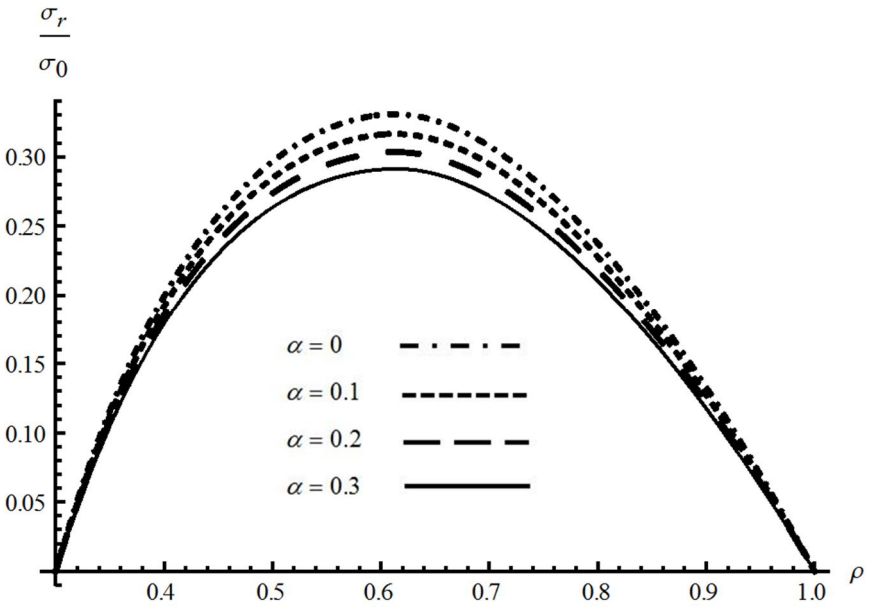

Figure 2 Variation of the radial stress with ρ in an a = 0.3 disk at the angular velocity corresponding to $\rho_c = 0.6$ for several α – values

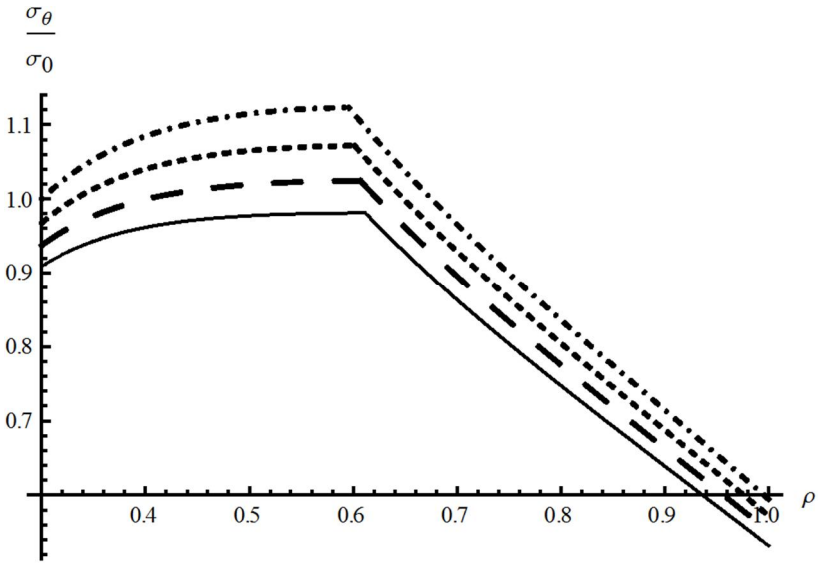

Figure 3 Variation of the circumferential stress with ρ in an a = 0.3 disk at the angular velocity corresponding to $\rho_c = 0.6$ for several α – values

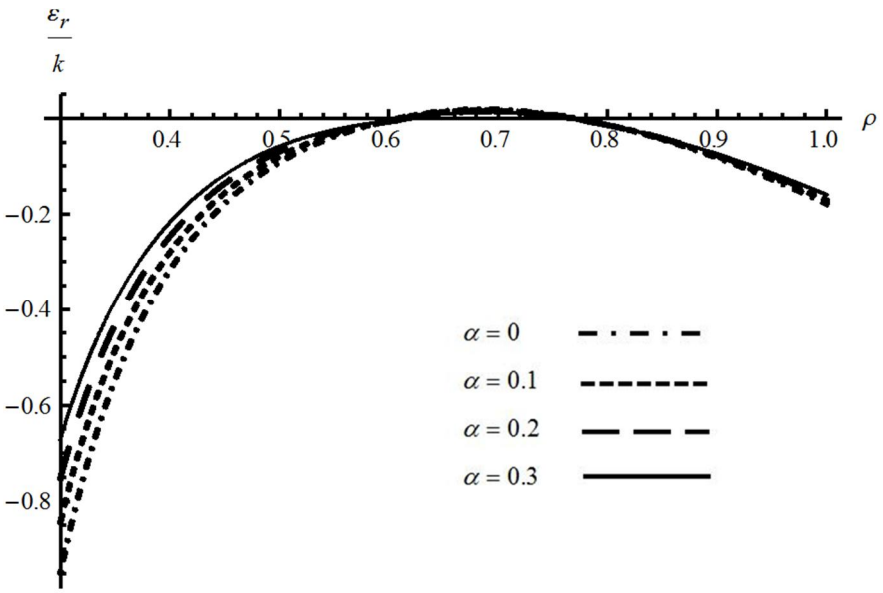

Figure 4 Variation of the total radial strain with ρ in an a = 0.3 disk at the angular velocity corresponding to $\rho_c = 0.6$ for several α – values

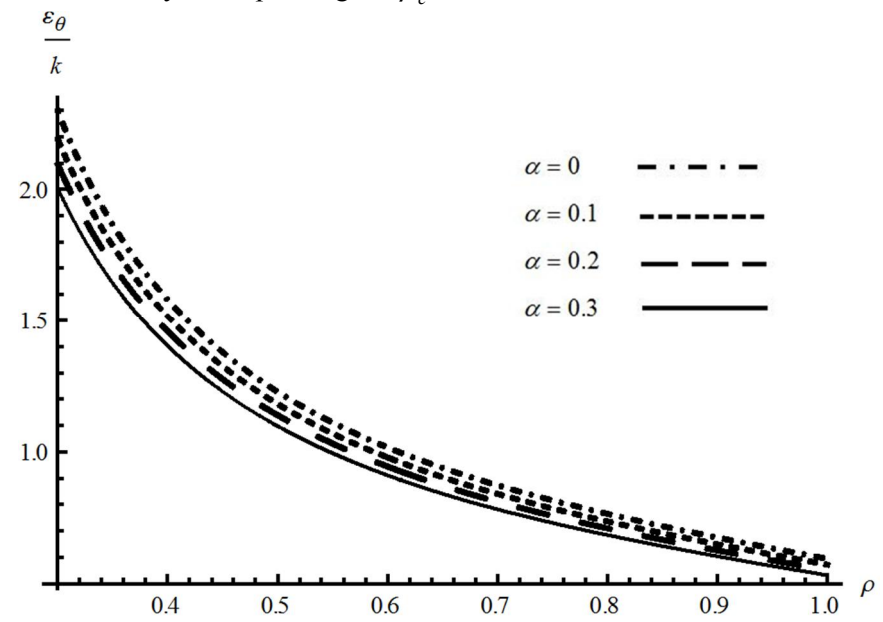

Figure 5 Variation of the total circumferential strain with ρ in an a = 0.3 disk at the angular velocity corresponding to $\rho_c = 0.6$ for several α – values

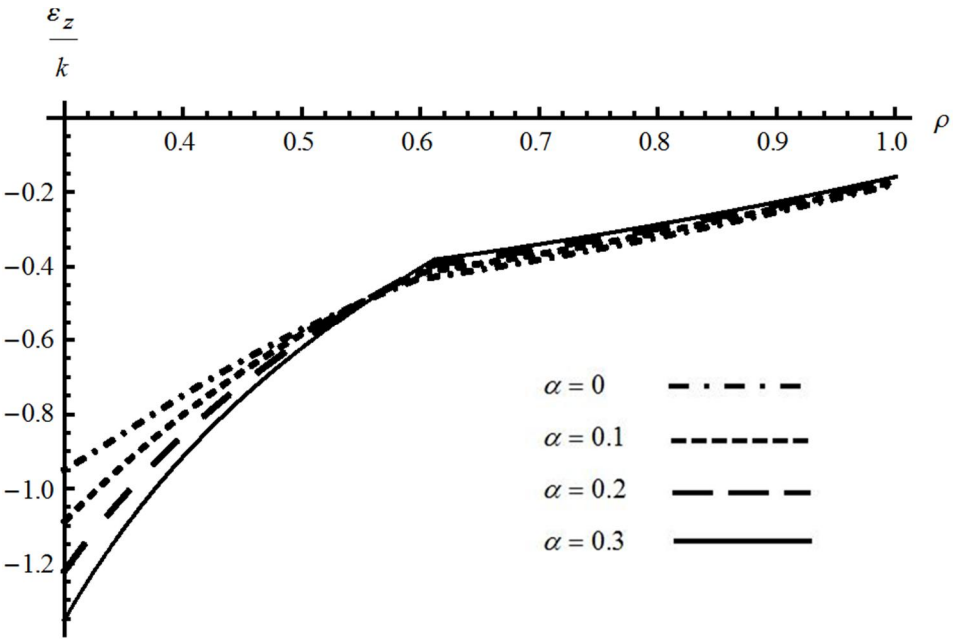

Figure 6 Variation of the total axial strain with ρ in an a = 0.3 disk at the angular velocity corresponding to $\rho_c = 0.6$ for several α – values

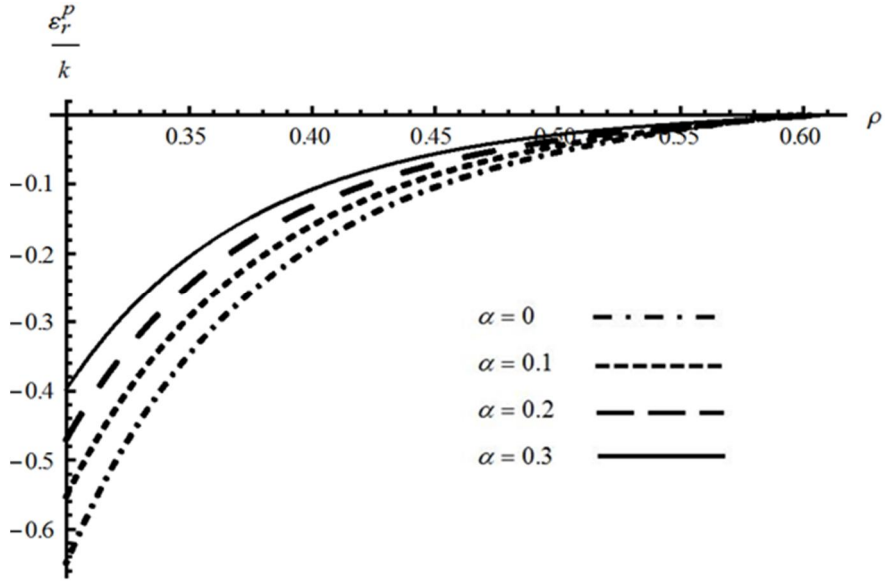

Figure 7 Variation of the radial plastic strain with ρ in an a = 0.3 disk at the angular velocity corresponding to $\rho_c = 0.6$ for several α – values

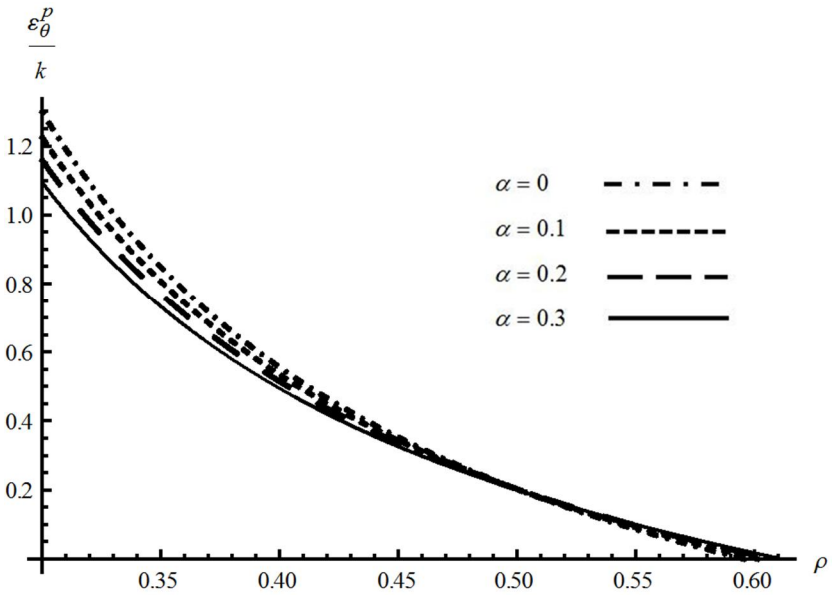

Figure 8 Variation of the circumferential plastic strain with ρ in an a = 0.3 disk at the angular velocity corresponding to $\rho_c = 0.6$ for several α – values

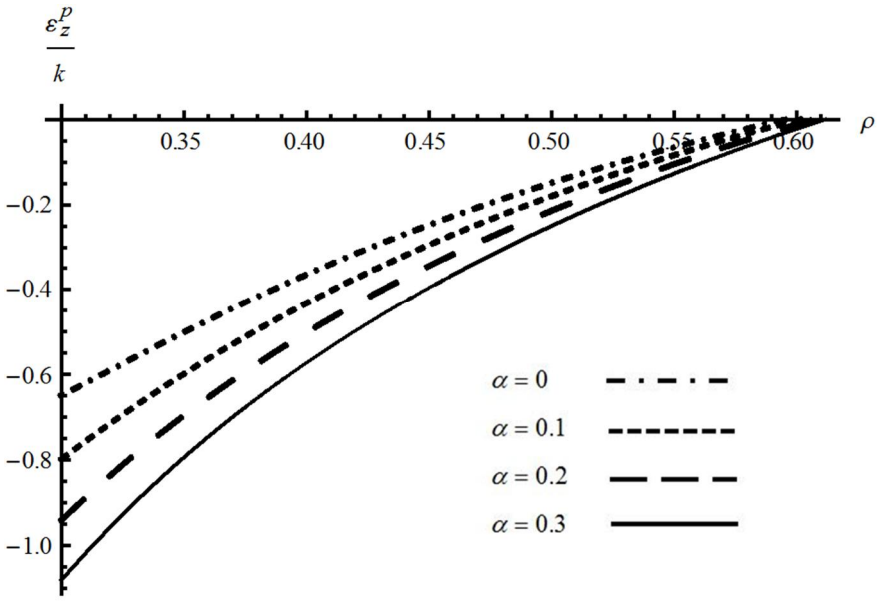

Figure 9 Variation of the axial plastic strain with ρ in an a = 0.3 disk at the angular velocity corresponding to $\rho_c = 0.6$ for several α – values

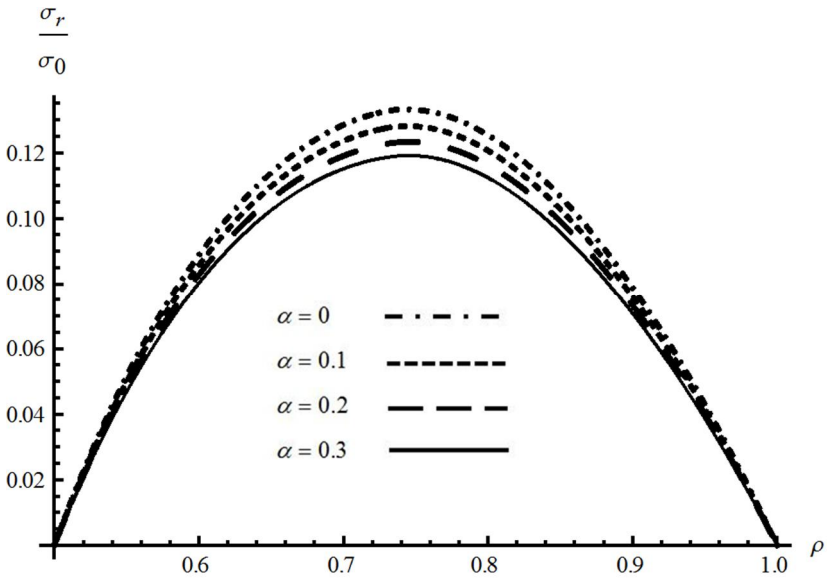

Figure 10 Variation of the radial stress with ρ in an a = 0.5 disk at the angular velocity corresponding to $\rho_c = 0.75$ for several $\alpha -$ values

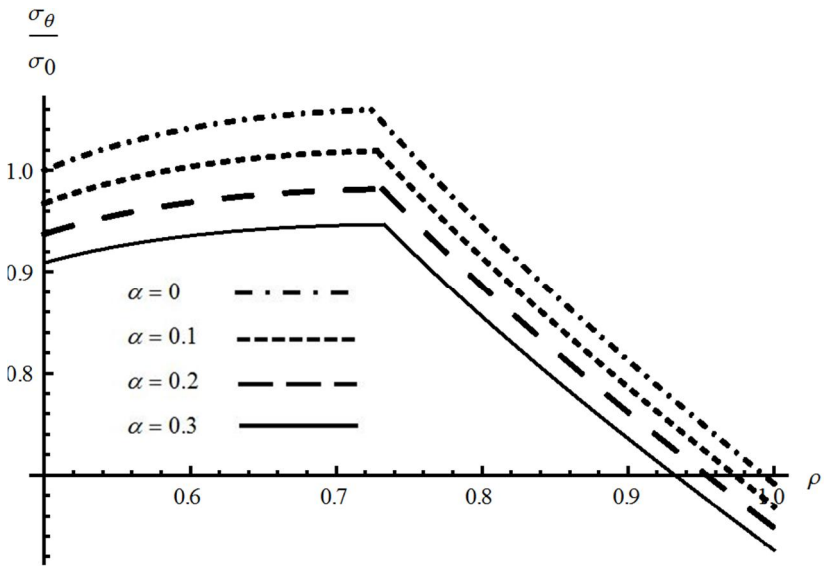

Figure 11 Variation of the circumferential stress with ρ in an a = 0.5 disk at the angular velocity corresponding to $\rho_c = 0.75$ for several $\alpha -$ values

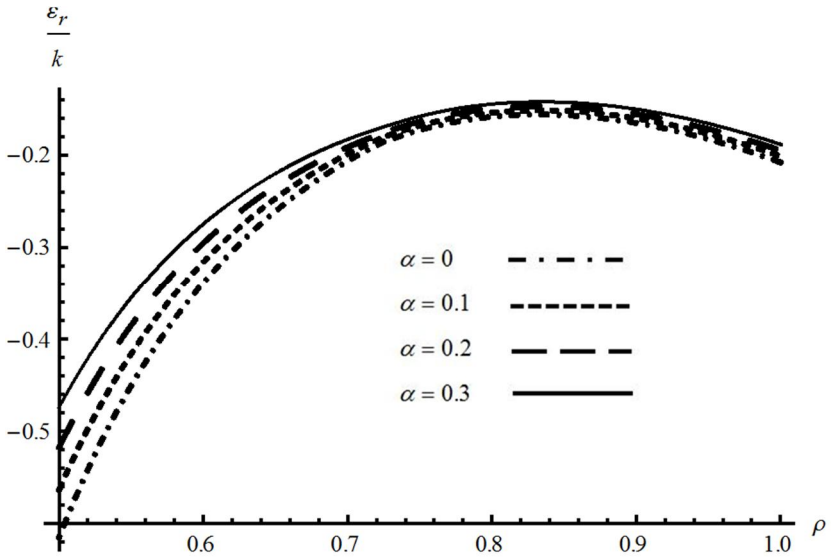

Figure 12 Variation of the total radial strain with ρ in an a = 0.5 disk at the angular velocity corresponding to $\rho_c = 0.75$ for several $\alpha -$ values

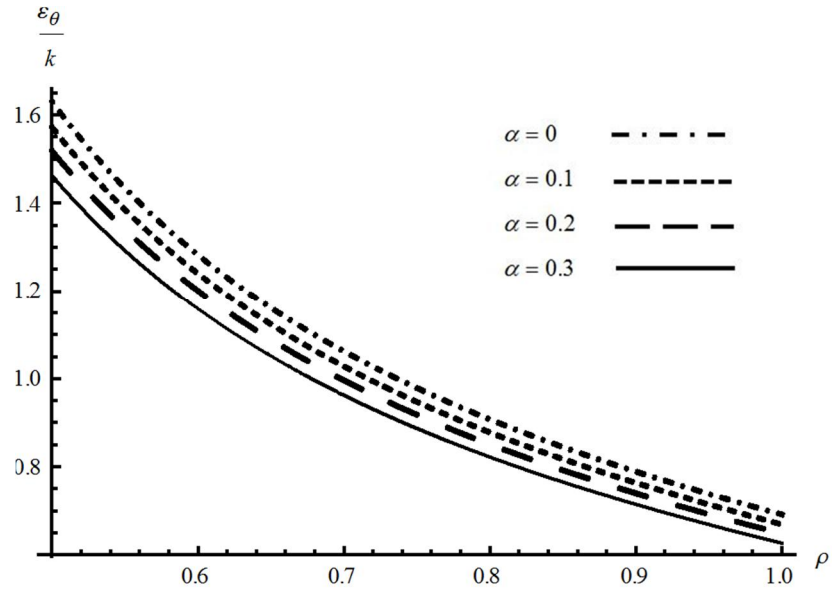

Figure 13 Variation of the total circumferential strain with ρ in an a = 0.5 disk at the angular velocity corresponding to $\rho_c = 0.75$ for several $\alpha -$ values

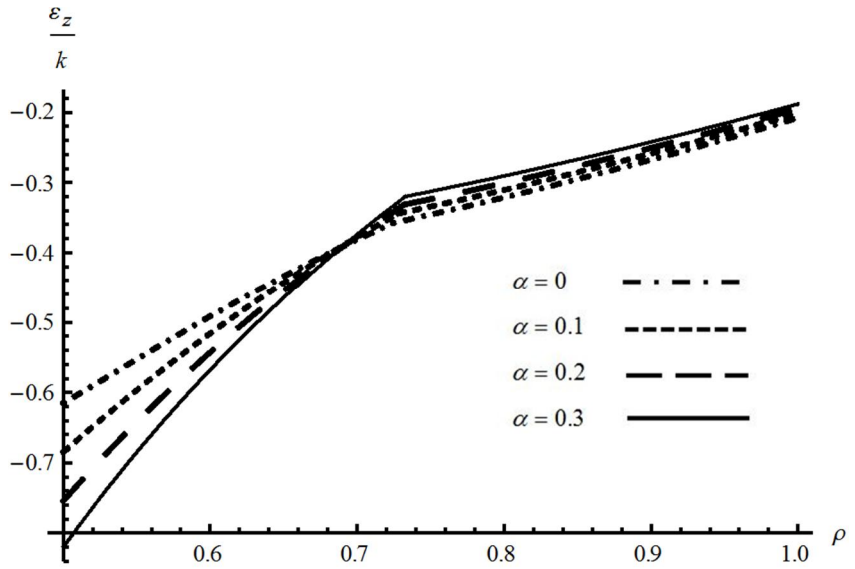

Figure 14 Variation of the total axial strain with ρ in an a = 0.5 disk at the angular velocity corresponding to $\rho_c = 0.75$ for several $\alpha -$ values

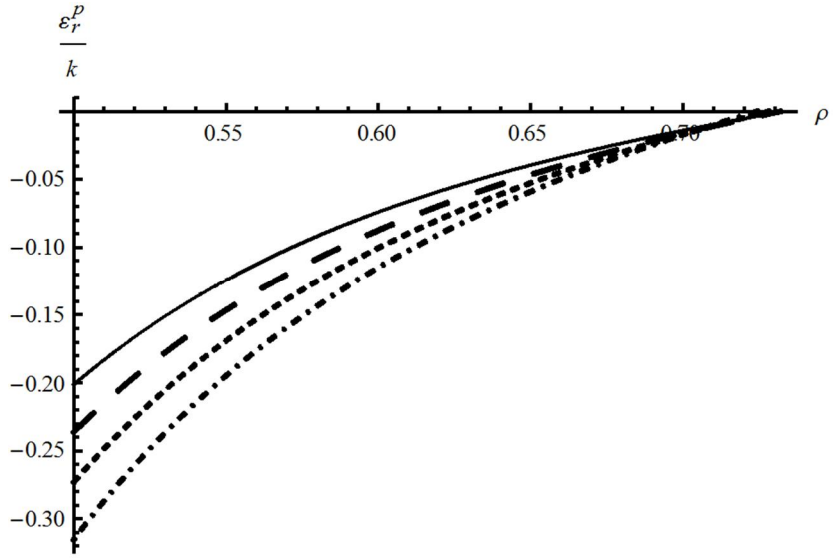

Figure 15 Variation of the radial plastic strain with ρ in an a = 0.5 disk at the angular velocity corresponding to $\rho_c = 0.75$ for several $\alpha -$ values

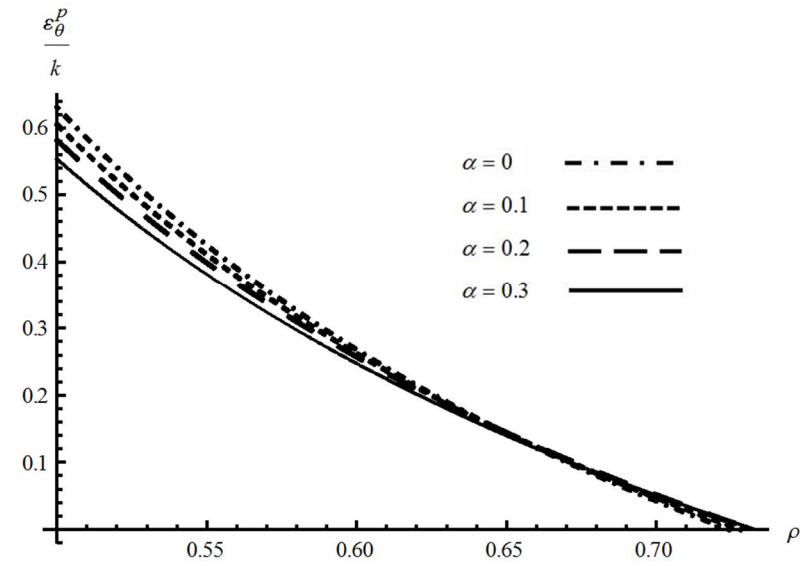

Figure 16 Variation of the circumferential plastic strain with ρ in an a = 0.5 disk at the angular velocity corresponding to $\rho_c = 0.75$ for several $\alpha -$ values

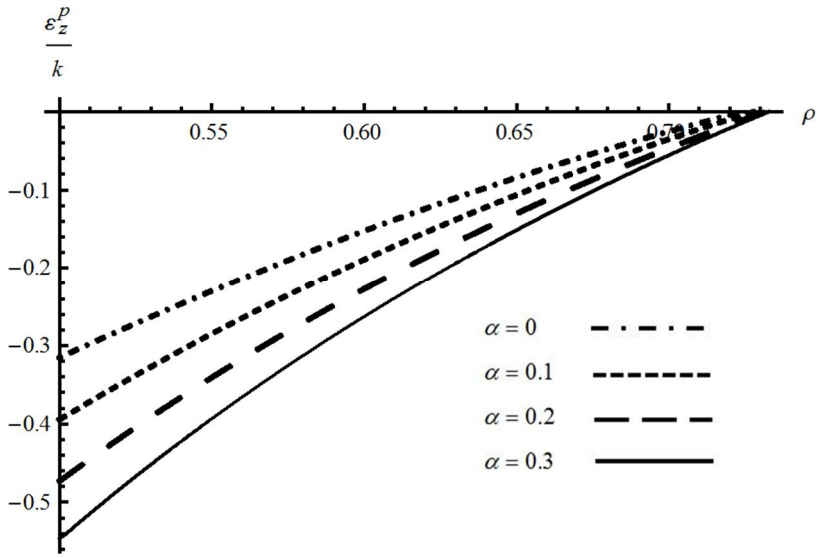

Figure 17 Variation of the axial plastic strain with ρ in an a = 0.5 disk at the angular velocity corresponding to $\rho_c = 0.75$ for several $\alpha -$ values

Chapter 3. Disk of variable thickness

3.1 Statement of the problem

Consider a thin annual rotating disc of variable thickness. It is assumed that the outer and inner radii of the disc are stress free. These radii are denoted by a_0 and b_0, respectively (Fig.18). It is convenient to introduce a cylindrical coordinate system (r, θ, z) whose $z-$ axis coincides with the axis of symmetry of the disc. Let σ_r, σ_θ and σ_z be the normal stresses in this coordinate system. Symmetry of the problem dictates that these stresses are the principal stresses. Moreover, $\sigma_z = 0$ under plane stress conditions. In the cylindrical coordinate system the boundary conditions are written as

$$\sigma_r = 0 \tag{3.1.1}$$

for $r = a_0$ and $r = b_0$. The only non-trivial equilibrium equation is (Timoshenko and Goodier, 1970)

$$\frac{d}{dr}\left(hr\sigma_r\right)-h\sigma_\theta+h\varsigma\omega^2r^2=0 \tag{3.1.2}$$

where ς is the material density, and ω is the angular velocity of the disc about the $z-$ axis. The thickness of the disc is assumed to vary according to the equation

$$h=h_0\left(\frac{r}{a_0}\right)^m \tag{3.1.3}$$

where h_0 is the thickness at the edge of the disc and m is a constant. This dependence of the thickness on the radius is of practical importance (Guven 1998, You *et al*. 2000, Hojjati and Hassani 2008). Substituting Eq. (3.1.3) into Eq. (3.1.2) yields

$$\frac{d\sigma_r}{dr}+\frac{\left(m+1\right)\sigma_r-\sigma_\theta}{r}+\varsigma\omega^2r=0\,. \tag{3.1.4}$$

Since $\sigma_z=0$, the Hooke's law in the cylindrical coordinate system reads

$$\varepsilon_r^e=\frac{\sigma_r-\nu\sigma_\theta}{E},\quad \varepsilon_\theta^e=\frac{\sigma_\theta-\nu\sigma_r}{E},\quad \varepsilon_z^e=-\frac{\nu\left(\sigma_r+\sigma_\theta\right)}{E}\,. \tag{3.1.5}$$

Here ν is Poisson's ratio and E is Young's modulus. The superscript e denotes the elastic part of the strain. Since the boundary value problem is statically determinate, no

relation between stress and plastic strain (or plastic strain rate) is required for stress analysis. Under plane stress conditions the yield criterion proposed in Drucker and Prager (1952) becomes

$$\frac{\alpha}{3}\left(\sigma_r+\sigma_\theta\right)+\sqrt{\sigma_\theta^2+\sigma_r^2-\sigma_r\sigma_\theta}=\sigma_0 \tag{3.1.6}$$

where α and σ_0 are material constants. It is worthy of note that this yield criterion adequately describes yielding of many metallic materials (Spitzig *et al*. 1976, Kao *et al*. 1990, Wilson 2002, Liu 2006). It is seen from Eq. (3.1.6) that the value of α controls the deviation of the pressure-dependent yield criterion adopted from the von Mises yield criterion and that the yield criterion (3.1.6) becomes the von Mises yield criterion at $\alpha=0$. It is convenient to rewrite (3.1.6) in the form

$$\left(1-\frac{\alpha^2}{9}\right)\sigma_r^2+\left(1-\frac{\alpha^2}{9}\right)\sigma_\theta^2-\left(1+\frac{2\alpha^2}{9}\right)\sigma_r\sigma_\theta+\frac{2\alpha}{3}\sigma_0\left(\sigma_r+\sigma_\theta\right)=\sigma_0^2 \tag{3.1.7}$$

and to introduce the following dimensionless quantities

$$\Omega=\frac{\varsigma\omega^2b_0^2}{\sigma_0},\quad a=\frac{a_0}{b_0},\quad \rho=\frac{r}{b_0}. \tag{3.1.8}$$

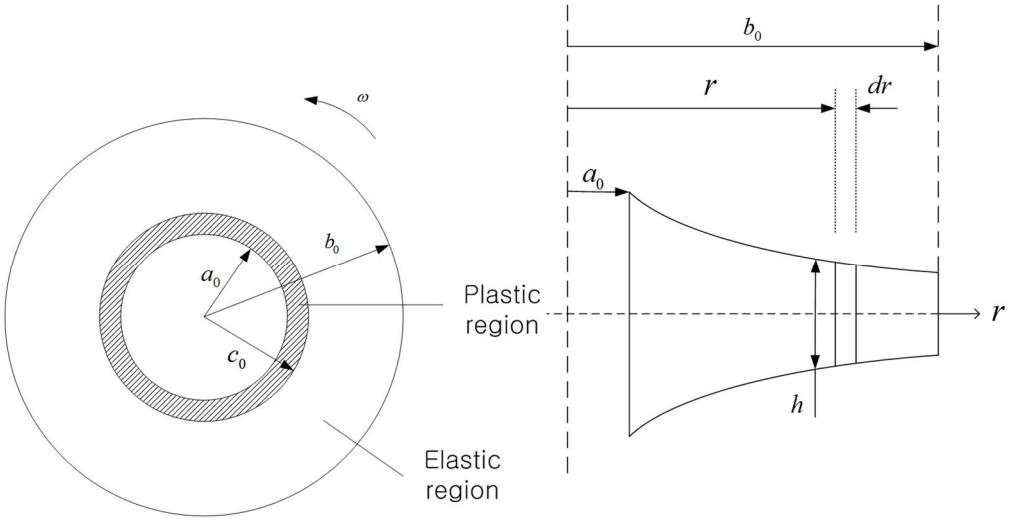

Fig. 18 Disc configuration

3.2 Solution

3.2.1 Purely elastic solution

The entire disc is elastic if Ω is small enough. The general solution of Eqs. (3.1.4) and (3.1.5) supplemented with the equation of strain compatibility is well known (see, for example, Timoshenko and Goodier 1970). In particular, the radial distribution of stress is given by

$$\frac{\sigma_r}{\sigma_0} = A\rho^{n_1} + B\rho^{n_2} + \Omega D_1 \rho^2 \quad , \quad \frac{\sigma_\theta}{\sigma_0} = A\left(m+1+n_1\right)\rho^{n_1} + B\left(m+1+n_2\right)\rho^{n_2} + \Omega D_2 \rho^2 \qquad (3.1.9)$$

where $n_1 = \dfrac{-(m+2)+\sqrt{(m+2)^2 - 4m(1+\nu)}}{2}$, $n_2 = \dfrac{-(m+2)-\sqrt{(m+2)^2 - 4m(1+\nu)}}{2}$,

$$D_1 = \frac{3+\nu}{1+3\nu-(3+\nu)(3+m)} \quad , \quad D_2 = \frac{3\nu+1}{1+3\nu-(3+\nu)(3+m)} .$$

Here A and B are constants of integration. In the case of purely elastic discs the solution (3.1.9) should satisfy the boundary conditions (3.1.1). Therefore,

$$A = A_e = \frac{a^{n_2} - a^2}{a^{n_1} - a^{n_2}} D_1 \Omega, \quad B = B_e = -\frac{a^{n_1} - a^2}{a^{n_1} - a^{n_2}} D_1 \Omega \quad . \tag{3.1.10}$$

Substitution of Eq. (3.1.10) into Eq. (3.1.9) provides the stress distribution in the purely elastic disc in the form

$$\begin{aligned} \frac{\sigma_r}{\sigma_0} &= \left[\left(\frac{a^{n_2} - a^2}{a^{n_1} - a^{n_2}} \right) \rho^{n_1} - \left(\frac{a^{n_1} - a^2}{a^{n_1} - a^{n_2}} \right) \rho^{n_2} + \rho^2 \right] D_1 \Omega, \\ \frac{\sigma_\theta}{\sigma_0} &= \left[D_1 \left(\frac{a^{n_2} - a^2}{a^{n_1} - a^{n_2}} \right) (m + 1 + n_1) \rho^{n_1} - D_1 \left(\frac{a^{n_1} - a^2}{a^{n_1} - a^{n_2}} \right) (m + 1 + n_2) \rho^{n_2} + D_2 \rho^2 \right] \Omega. \end{aligned} \tag{3.1.11}$$

The plastic yielding is assumed to begin at $\rho = a$ and this assumption should be verified *a posteriori*. Since $\sigma_r = 0$ at $\rho = a$, it follows from Eq. (3.1.7) that

$$\frac{\sigma_\theta}{\sigma_0} = \frac{3}{\alpha + 3} \tag{3.1.12}$$

at $\rho = a$ on the initiation of plastic yielding. Replacing ρ in Eq. (3.1.11) with a and eliminating σ_θ / σ_0 with the use of Eq. (3.1.12) yield

$$\Omega_e = \frac{3}{(\alpha + 3)} \left[D_1 \left(\frac{a^{n_2} - a^2}{a^{n_1} - a^{n_2}} \right) (m + 1 + n_1) a^{n_1} - D_1 \left(\frac{a^{n_1} - a^2}{a^{n_1} - a^{n_2}} \right) (m + 1 + n_2) a^{n_2} + D_2 a^2 \right]^{-1} \tag{3.1.13}$$

where Ω_e is the value of Ω corresponding to the initiation of plastic yielding.

3.2.2 Elastic/Plastic stress solution

Plastic yielding occurs in the disc if $\Omega_e \le \Omega$. Let Ω_p be the angular velocity at which the whole disc plastic. If $\Omega_e < \Omega < \Omega_p$ then the disc has an inner plastic part, $a \le \rho \le \rho_c$ (or $a_0 \le r \le c_0$), and an outer elastic part, $\rho_c \le \rho \le 1$ (or $c_0 \le r \le b_0$). Here c_0 is the radius of the plastic/elastic boundary and $\rho_c = c_0/b_0$ is its dimensionless representation (Fig. 18). The general solution (3.1.9) is valid in the elastic region. However, *A* and *B* are not given by Eq. (3.1.10). This solution should satisfy the boundary condition (3.1.1) at $\rho = 1$. Therefore,

$$A + B + \Omega D_1 = 0. \tag{3.1.14}$$

In the plastic region, it is necessary to solve Eqs. (3.1.4) and (3.1.7). The yield criterion (3.1.7) is satisfied by the following substitution (Alexandrov *et al*., 2011)

$$\begin{aligned}
&\frac{\sigma_r}{\sigma_0} = 3\beta_0 - \frac{\beta_1}{2}\left(1 + 3\sqrt{3}\beta_1\right)\sin\psi + \frac{\sqrt{3}}{2}\beta_1\left(1 - \sqrt{3}\beta_1\right)\cos\psi,\\
&\frac{\sigma_\theta}{\sigma_0} = 3\beta_0 + \frac{\beta_1}{2}\left(1 - 3\sqrt{3}\beta_1\right)\sin\psi - \frac{\sqrt{3}}{2}\beta_1\left(1 + \sqrt{3}\beta_1\right)\cos\psi,\\
&\beta_0 = \frac{2\alpha}{4\alpha^2 - 9}, \quad \beta_1 = \frac{\sqrt{3}}{\sqrt{9 - 4\alpha^2}}.
\end{aligned} \tag{3.1.15}$$

Here ψ is a new function of ρ. Eliminating σ_r and σ_θ in Eq. (3.1.4) by means of Eq. (3.1.15) leads to

$$\begin{aligned}&\beta_1\rho\left[\left(1+3\sqrt{3}\beta_1\right)\cos\psi+\sqrt{3}\left(1-\sqrt{3}\beta_1\right)\sin\psi\right]\frac{\partial\psi}{\partial\rho}=\\&6\beta_0 m+\beta_1\left[-3\beta_1 m+\sqrt{3}\left(2+m\right)\right]\cos\psi-\beta_1\left(2+m+3\sqrt{3}\beta_1 m\right)\sin\psi+2\rho^2\Omega\ .\end{aligned}\tag{3.1.16}$$

This equation should be solved numerically. Let ψ_a be the value of ψ at $\rho=a$. Then, the boundary condition for Eq. (3.1.16) is

$$\psi=\psi_a\tag{3.1.17}$$

for $\rho=a$. The solution of Eq. (3.1.16) satisfying the boundary condition (3.1.17) is denoted as

$$\psi=\Psi\left(\rho,\Omega\right).\tag{3.1.18}$$

The second argument of the function $\Psi\left(\rho,\Omega\right)$ emphasizes that the solution depends on Ω. It follows from Eqs. (3.1.15) that

$$\frac{\sigma_\theta-\sigma_r}{\sigma_0}=\frac{2\sqrt{3}}{\sqrt{9-4\alpha^2}}\sin\left(\psi-\frac{\pi}{3}\right),\quad\frac{\sigma_\theta+\sigma_r}{\sigma_0}=\frac{12\alpha}{4\alpha^2-9}+\frac{18}{\left(4\alpha^2-9\right)}\sin\left(\psi+\frac{\pi}{6}\right).\tag{3.1.19}$$

It is reasonable to assume that $\sigma_\theta > \sigma_r$. Then, it is seen from Eq. (3.1.19) that

$$\frac{\pi}{3} < \psi < \frac{4\pi}{3} \quad . \tag{3.1.20}$$

The boundary condition (3.1.1) at $\rho = a$ and Eq. (3.1.15) for σ_r combine to give

$$\psi_a = \frac{4\pi}{3} - \arcsin q, \quad q = \frac{\sqrt{3}\sqrt{9-4\alpha^2}}{2\left(3+\alpha\right)}. \tag{3.1.21}$$

The inequality (3.1.20) has been here taken into account. The disc becomes fully plastic when $\rho_c = 1$. It follows from the boundary condition (3.1.1) at $r = b_0$ (or $\rho = 1$) that $\psi_c = \psi_a$ at this instant. Therefore, Ω_p is determined by the condition

$$\frac{4\pi}{3} - \arcsin q = \Psi\left(1, \Omega_p\right). \tag{3.1.22}$$

Let ψ_c be the value of ψ at $\rho = \rho_c$. The radial and circumferential stresses must be continuous across the plastic/elastic boundary. Then, it follows from Eqs. (3.1.9), (3.1.14), (3.1.18) and (3.1.19) that

$$
\begin{aligned}
&B\left[\left(m+n_2\right)\rho_c^{n_2}-\left(m+n_1\right)\rho_c^{n_1}\right]+\left[\left(D_2-D_1\right)\rho_c^2-D_1\left(m+n_1\right)\rho_c^{n_1}\right]\Omega=\\
&\frac{2\sqrt{3}}{\sqrt{9-4\alpha^2}}\sin\left(\Psi\left(\rho_c,\Omega\right)-\frac{\pi}{3}\right),\\
&B\left[\left(m+2+n_2\right)\rho_c^{n_2}-\left(m+2+n_1\right)\rho_c^{n_1}\right]+\left[\left(D_2+D_1\right)\rho_c^2-D_1\left(m+2+n_1\right)\rho_c^{n_1}\right]\Omega=\\
&=\frac{12\alpha}{4\alpha^2-9}+\frac{18}{4\alpha^2-9}\sin\left(\Psi\left(\rho_c,\Omega\right)+\frac{\pi}{6}\right).
\end{aligned}
\tag{3.1.23}
$$

Eliminating B between these two equations yields

$$
\begin{aligned}
&\left[\left(m+n_2\right)\rho_c^{n_2}-\left(m+n_1\right)\rho_c^{n_1}\right]\left\{\begin{array}{l}\dfrac{12\alpha}{4\alpha^2-9}+\dfrac{18}{4\alpha^2-9}\sin\left(\Psi\left(\rho_c,\Omega\right)+\dfrac{\pi}{6}\right)-\\ \left[\left(D_2+D_1\right)\rho_c^2-D_1\left(m+2+n_1\right)\rho_c^{n_1}\right]\Omega\end{array}\right\}=\\
&\left[\left(m+2+n_2\right)\rho_c^{n_2}-\left(m+2+n_1\right)\rho_c^{n_1}\right]\left\{\begin{array}{l}\dfrac{2\sqrt{3}}{\sqrt{9-4\alpha^2}}\sin\left(\Psi\left(\rho_c,\Omega\right)-\dfrac{\pi}{3}\right)-\\ \left[\left(D_2-D_1\right)\rho_c^2-D_1\left(m+n_1\right)\rho_c^{n_1}\right]\Omega\end{array}\right\}.
\end{aligned}
\tag{3.1.24}
$$

This equation supplies the dependence of ρ_c on Ω in implicit form. The variation of ψ_c with Ω is determined by substituting this dependence into Eq. (3.1.18). Then, the dependence of B on Ω can be found from any of Eqs. (3.1.23). Finally, the variation of A with Ω is given by Eq. (3.1.14).

Let Ω_f be the maximum angular velocity. It is assumed that $\Omega_e<\Omega_f<\Omega_p$ where Ω_p is determined from Eq. (3.1.22). Having found A, B, ρ_c and ψ_c as functions of Ω it is possible to calculate the values of these functions at $\Omega=\Omega_f$. Then, the distribution of σ_r and σ_θ is determined from Eq. (3.1.9) in the range $\rho_c\le\rho\le1$

and from Eqs. (3.1.15) and (3.1.18) in the range $a \le \rho \le \rho_c$. The latter is in parametric form with ψ being the parameter.

Typical values of *m* are $m = -0.5$ (Guven 1992) and $m = -0.25$ (Guven 1998). Using these values of m and $m = 0$ (constant thickness) calculation has been performed assuming that $\rho_c = 0.3$ and $\rho_c = 0.5$ in an $a = 0.2$ disc. In order to illustrate the effect of pressure-dependency of the yield criterion, two values of α have been chosen, $\alpha = 0$ (pressure-independent material) and $\alpha = 0.3$ (Liu 2006). It is assumed that $\nu = 0.3$. Table 1 shows the corresponding values of Ω_f. The effect of m - value on the distribution of the radial stress with ρ at $\rho_c = 0.3$ is illustrated in Fig.19 for $\alpha = 0$ and in Fig. 20 for $\alpha = 0.3$. It is seen from these figures that the radial stress increases as the value of m decreases. The same effect is seen for $\rho_c = 0.5$ in Fig. 21 for $\alpha = 0$ and in Fig. 22 for $\alpha = 0.3$. The effect of m - value on the circumferential stress is not so significant. In particular, the distribution of this stress component with ρ for $\rho_c = 0.3$ is depicted in Fig. 23 for $\alpha = 0$ and in Fig. 24 for $\alpha = 0.3$. In the case of $\rho_c = 0.5$ the variation of the circumferential stress with ρ is shown in Fig. 25 for $\alpha = 0$ and in Fig. 26 for $\alpha = 0.3$.

3.3 Residual stresses

It is assumed that unloading is purely elastic. This assumption should be verified a posteriori. The stress increments, $\Delta\sigma_r$ and $\Delta\sigma_\theta$, are calculated by Eqs. (3.1.9) and (3.1.10) where Ω should be replaced with $-\Omega_f$, A with ΔA, and B with ΔB when the angular velocity decreases from Ω_f to zero. As a result,

$$\Delta A=-\left(\frac{a^{n_2}-a^2}{a^{n_1}-a^{n_2}}\right)\frac{\Omega_f\left(3+\nu\right)}{\left[1+3\nu-\left(3+\nu\right)\left(3+m\right)\right]},$$
$$\Delta B=\left(\frac{a^{n_1}-a^2}{a^{n_1}-a^{n_2}}\right)\frac{\Omega_f\left(3+\nu\right)}{\left[1+3\nu-\left(3+\nu\right)\left(3+m\right)\right]},$$
$$\frac{\Delta\sigma_r}{\sigma_0}=\Delta A\rho^{n_1}+\Delta B\rho^{n_2}-\frac{\Omega_f\left(3+\nu\right)}{\left[1+3\nu-\left(3+\nu\right)\left(3+m\right)\right]}\rho^2, \tag{3.1.25}$$
$$\frac{\Delta\sigma_\theta}{\sigma_0}=\Delta A\left(m+1+n_1\right)\rho^{n_1}+\Delta B\left(m+1+n_2\right)\rho^{n_2}-\frac{\Omega_f\left(3\nu+1\right)}{\left[1+3\nu-\left(3+\nu\right)\left(3+m\right)\right]}\rho^2 .$$

Then, the residual stresses are

$$\frac{\sigma_r^{res}}{\sigma_0}=\frac{\sigma_r}{\sigma_0}+\frac{\Delta\sigma_r}{\sigma_0},\quad \frac{\sigma_\theta^{res}}{\sigma_0}=\frac{\sigma_\theta}{\sigma_0}+\frac{\Delta\sigma_\theta}{\sigma_0}. \tag{3.1.26}$$

Here σ_r and σ_θ are found from the solution given in Section 3.2.1 at $\Omega=\Omega_f$ (Figs. 19 – 26). Using Eq. (3.1.7) the condition of the validity of the purely elastic solution at unloading can be written as

$$\left(1-\frac{\alpha^2}{9}\right)\left(\frac{\sigma_r^{res}}{\sigma_0}\right)^2+\left(1-\frac{\alpha^2}{9}\right)\left(\frac{\sigma_\theta^{res}}{\sigma_0}\right)^2- -\left(1+\frac{2\alpha^2}{9}\right)\frac{\sigma_r^{res}}{\sigma_0}\frac{\sigma_\theta^{res}}{\sigma_0}+\frac{2\alpha}{3}\left(\frac{\sigma_r^{res}}{\sigma_0}+\frac{\sigma_\theta^{res}}{\sigma_0}\right)-1\le 0. \tag{3.1.27}$$

Using Eqs. (3.1.25) and (3.1.26) the distribution of the residual stress has been calculated. The effect of m - value on the distribution of the radial residual stress with ρ at $\rho_c=0.3$ is illustrated in Fig.27 for $\alpha=0$ and in Fig. 28 for $\alpha=0.3$. It is seen from these figures that the effect is negligible at this value of ρ_c. A larger effect is

revealed at $\rho_c = 0.5$. It is seen from Fig. 29 for $\alpha = 0$ and in Fig. 30 for $\alpha = 0.3$. In both cases $\left|\sigma_r^{res}\right|$ increases as the value of m increases. The effect of m - value on the circumferential residual stress is also insignificant for $\rho_c = 0.3$. It is seen in Fig.31 for $\alpha = 0$ and in Fig. 32 for $\alpha = 0.3$. In the case of $\rho_c = 0.5$ the variation of the circumferential residual stress with ρ is shown in Fig. 33 for $\alpha = 0$ and in Fig. 34 for $\alpha = 0.3$. It is seen from these figures that the effect of m-value of the circumferential residual stress is more pronounced in the plastic region. It is also seen that the dependence of σ_θ^{res} on m at a given value of ρ is not monotonic.

The distributions of the residual stresses shown in Figs. 27 to 34 have been substituted into Eq. (3.1.27) to verify that the yield criterion is not violated in the elastic region.

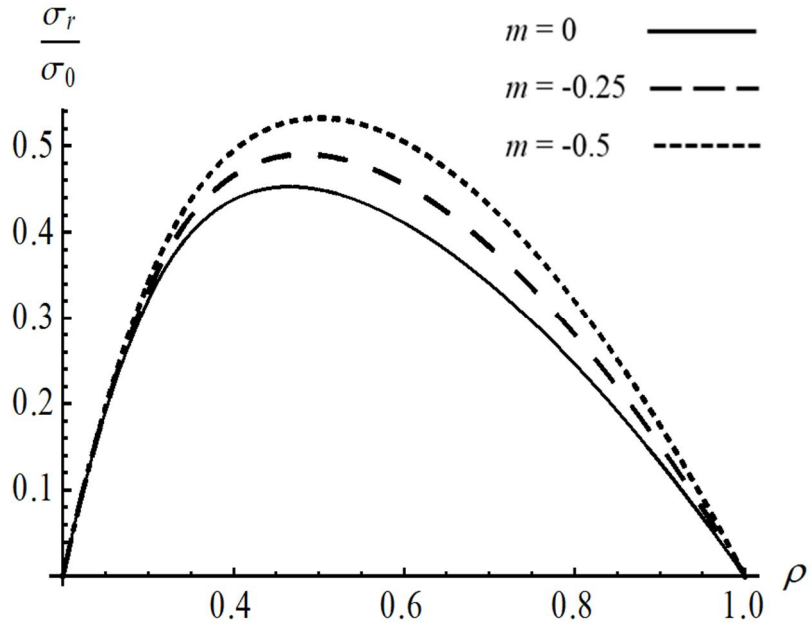

Figure 19 Variation of the radial stress with ρ at $\rho_c = 0.3$, $\alpha = 0$, and several m – values

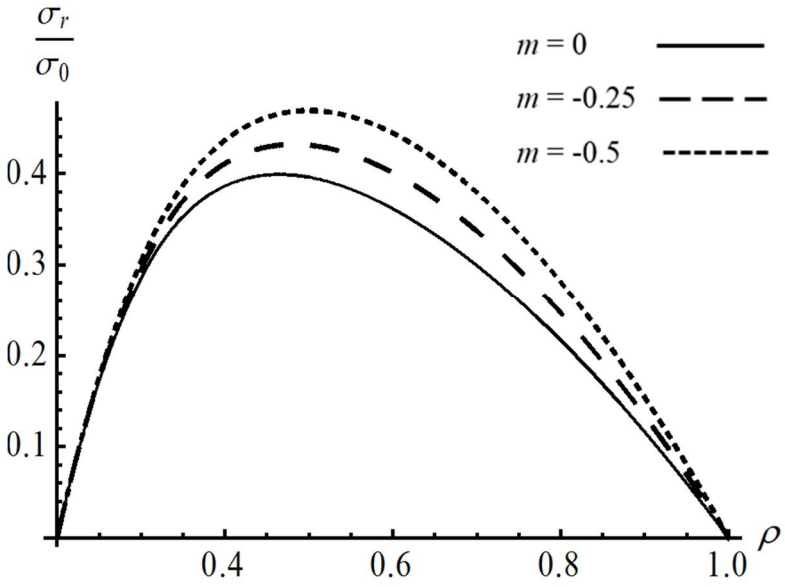

Figure 20 Variation of the radial stress with ρ at $\rho_c = 0.3$, $\alpha = 0.3$, and several m – values

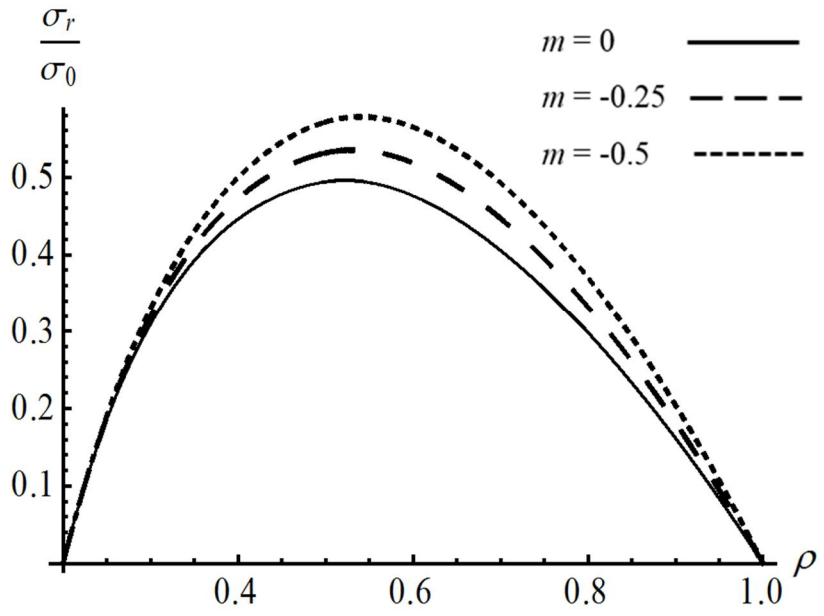

Figure 21 Variation of the radial stress with ρ at $\rho_c = 0.5$, $\alpha = 0$, and several m – values

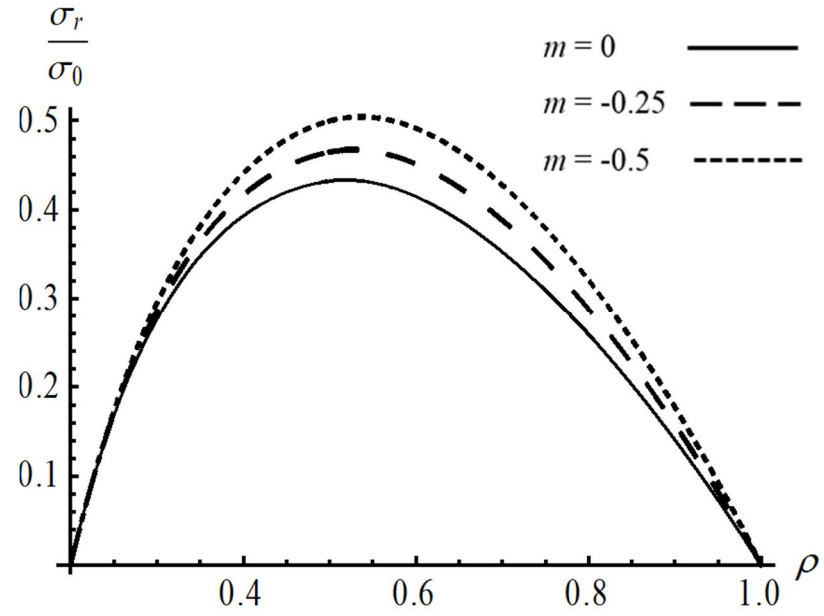

Figure 22 Variation of the radial stress with ρ at $\rho_c = 0.5$, $\alpha = 0.3$, and several m – values

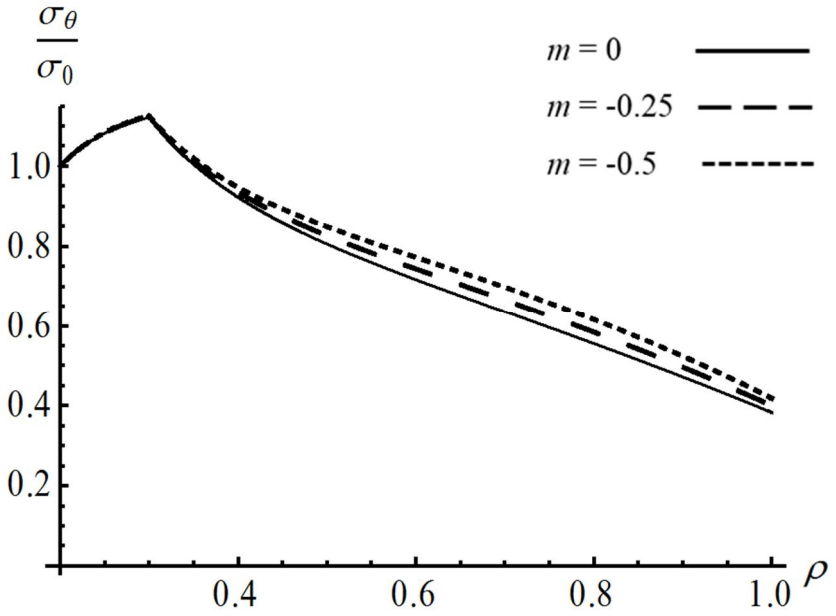

Figure 23 Variation of the circumferential stress with ρ at $\rho_c = 0.3$, $\alpha = 0$, and several m – values

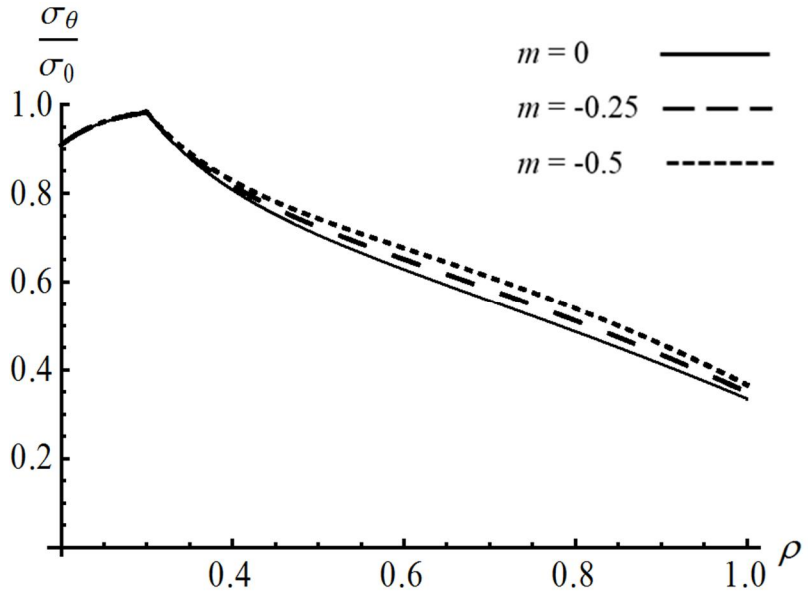

Figure 24 Variation of the circumferential stress with ρ at $\rho_c = 0.3$, $\alpha = 0.3$, and several m – values

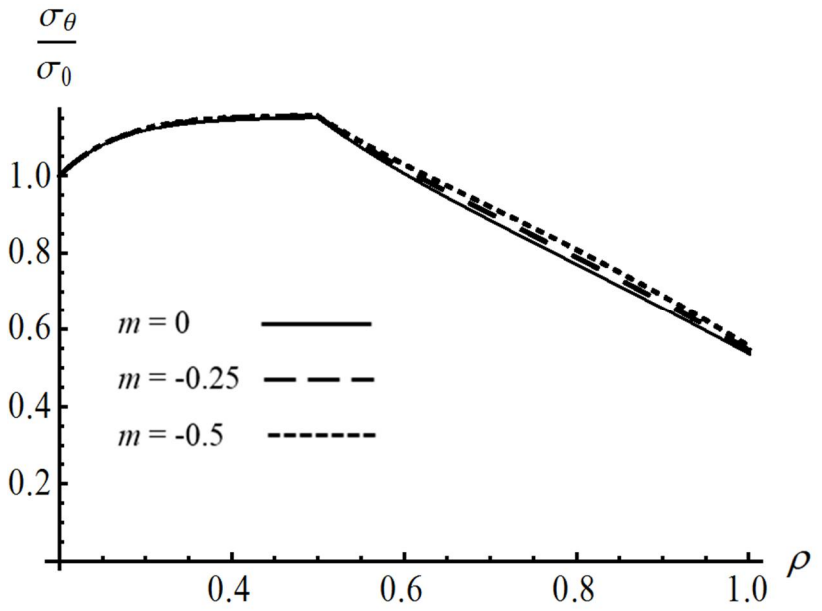

Figure 25 Variation of the circumferential stress with ρ at $\rho_c = 0.5$, $\alpha = 0$, and several m – values

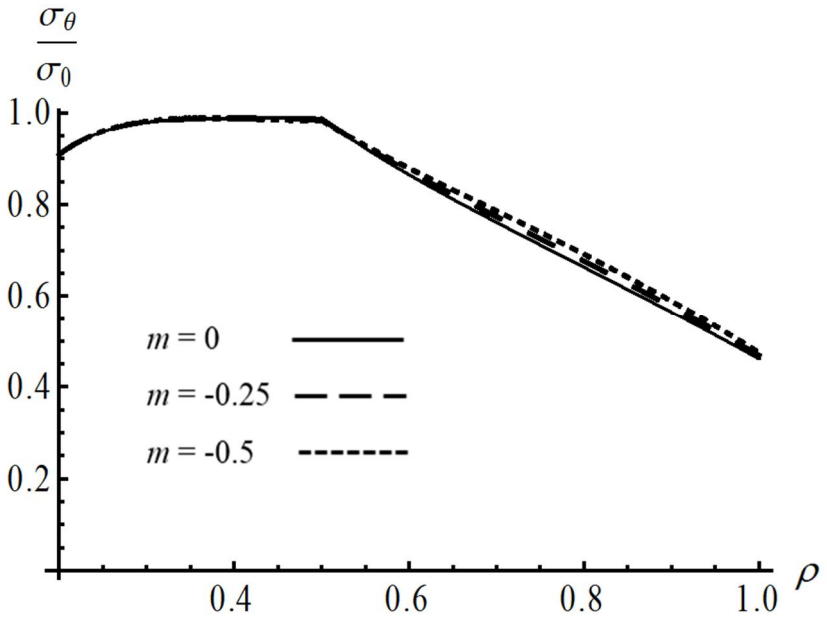

Figure 26 Variation of the circumferential stress with ρ at $\rho_c = 0.5$, $\alpha = 0.3$, and several m – values

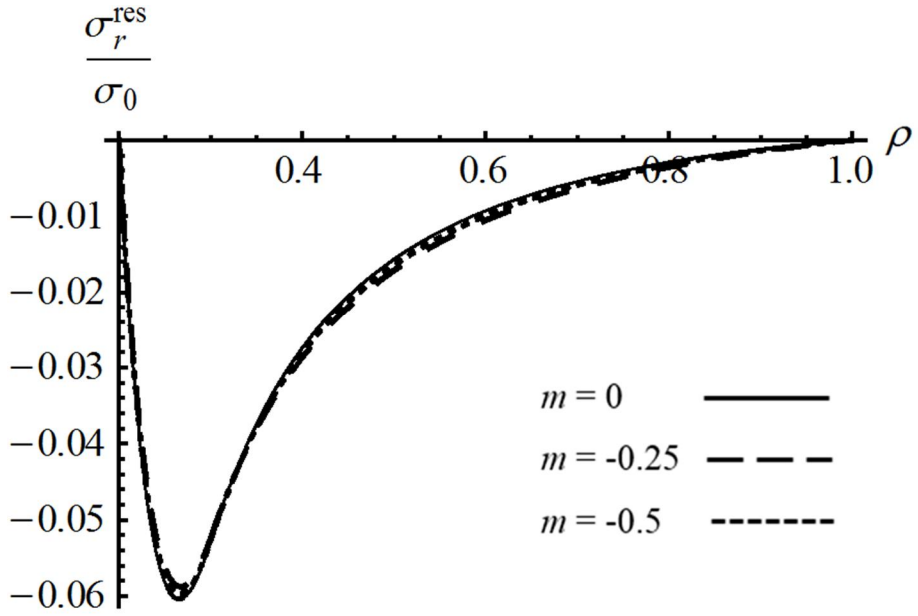

Figure 27 Variation of the residual radial stress with ρ at $\rho_c = 0.3$, $\alpha = 0$, and several m – values

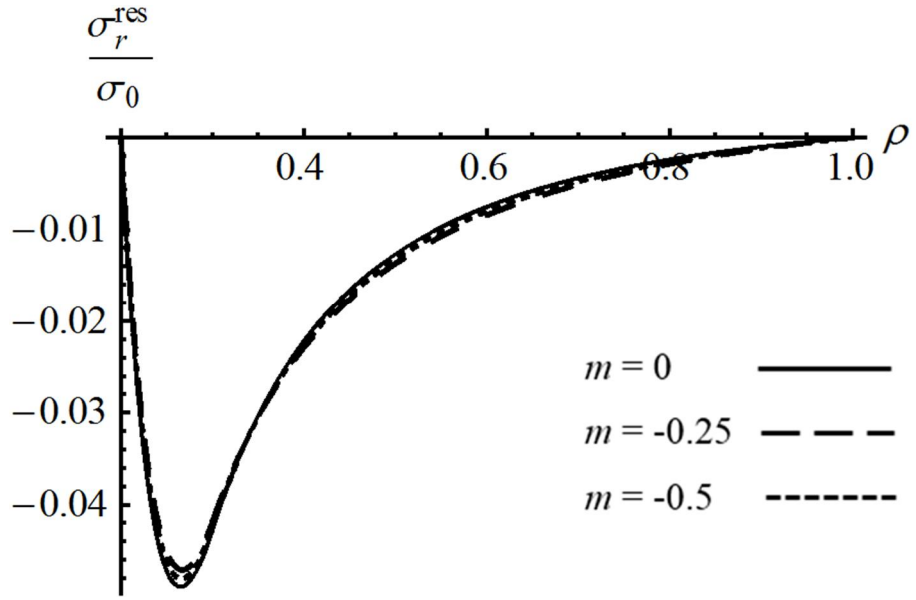

Figure 28 Variation of the residual radial stress with ρ at $\rho_c = 0.3$, $\alpha = 0.3$, and several m – values

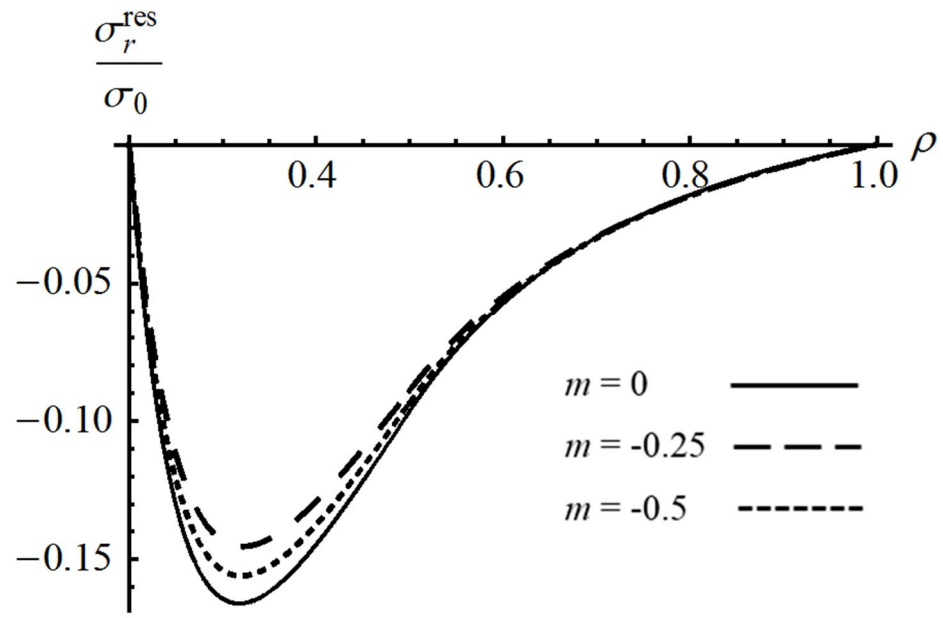

Figure 29 Variation of the residual radial stress with ρ at $\rho_c = 0.5$, $\alpha = 0$, and several m – values

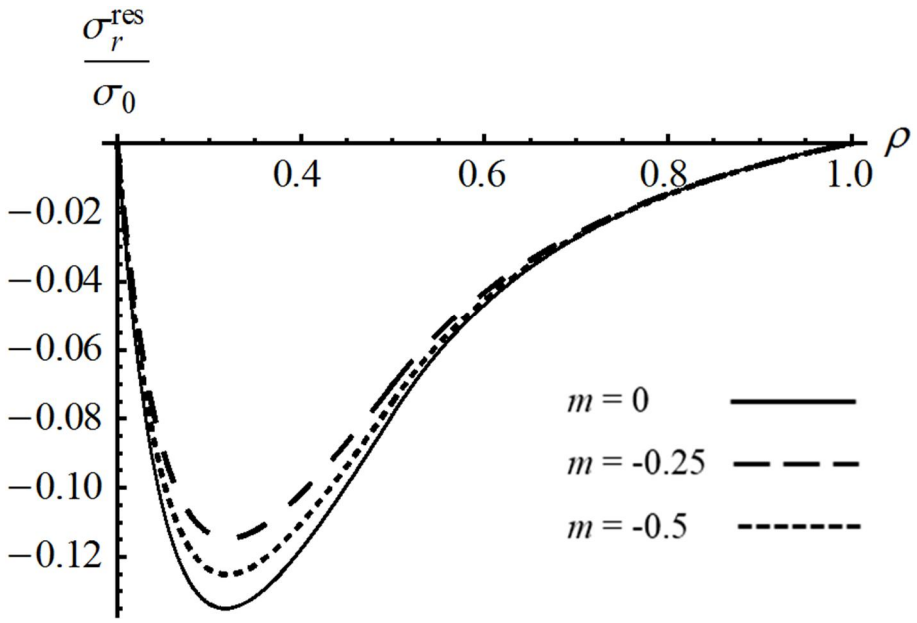

Figure 30 Variation of the residual radial stress with ρ at $\rho_c = 0.5$, $\alpha = 0.3$, and several m – values

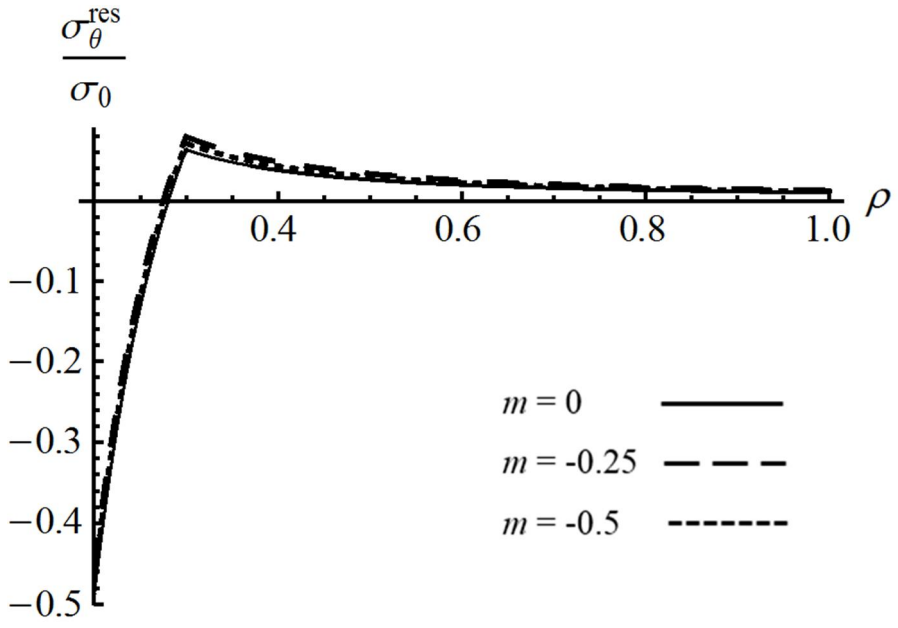

Figure 31 Variation of the residual circumferential stress with ρ at $\rho_c = 0.3$, $\alpha = 0$, and several $m-$values

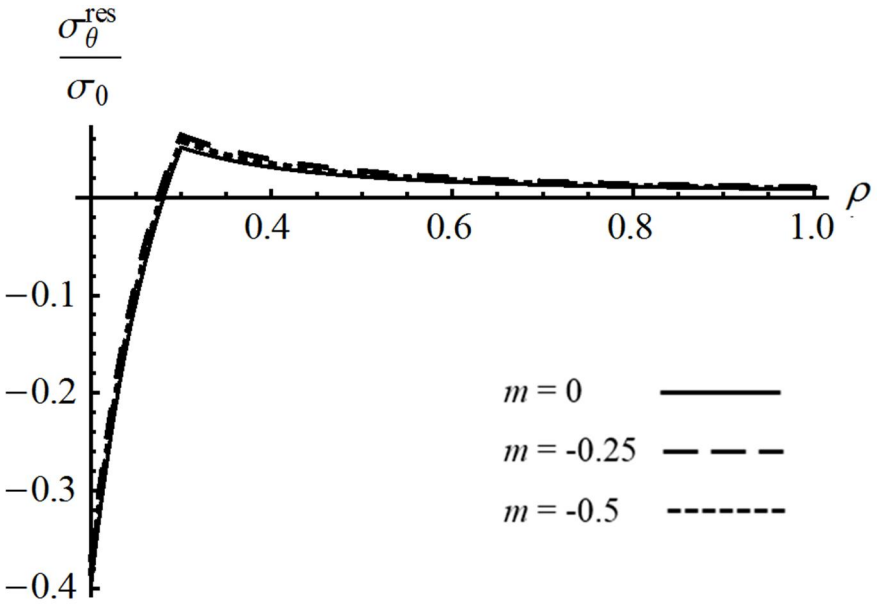

Figure 32 Variation of the residual circumferential stress with ρ at $\rho_c = 0.3$, $\alpha = 0.3$, and several $m-$values

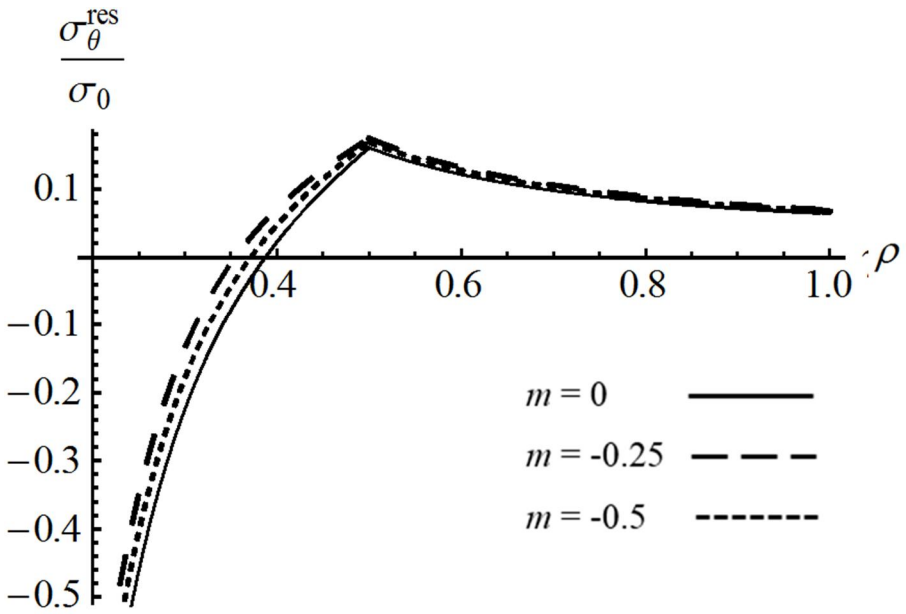

Figure 33 Variation of the residual circumferential stress with ρ at $\rho_c = 0.5$,

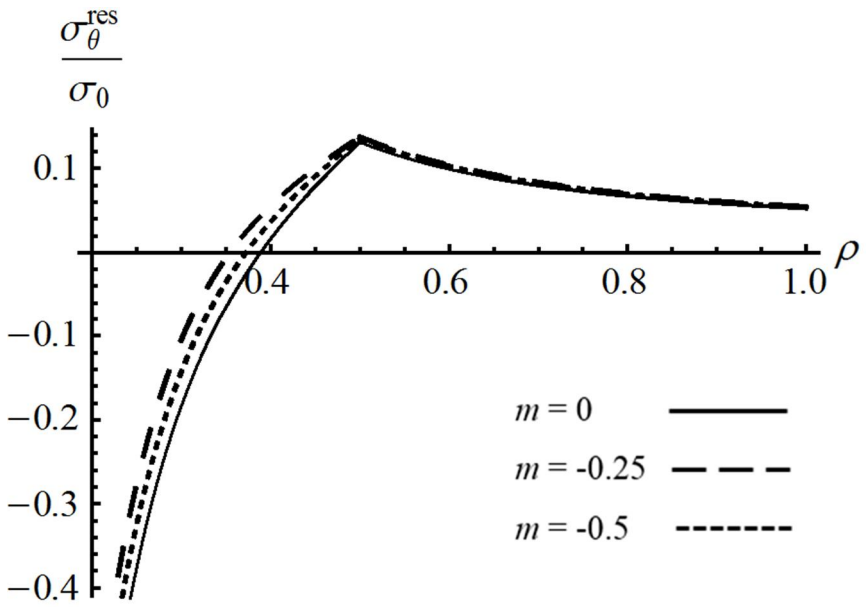

$\alpha = 0$ and several $m-$values

Figure 34 Variation of the residual circumferential stress with ρ at $\rho_c = 0.5$,

$\alpha = 0.3$, and several $m-$ values

Chapter 4. Validation of model

The original system of equations is

$$\frac{\partial \sigma_r}{\sigma_0 \partial \rho} + \frac{\sigma_r - \sigma_\theta}{\sigma_0 \rho} = -\frac{\Omega \rho}{\sqrt{3}},$$

(4.1.1)

$$\left(1 - \frac{\alpha^2}{9}\right)\left(\sigma_r^2 + \sigma_\theta^2\right) - \left(1 + \frac{2\alpha^2}{9}\right)\sigma_r \sigma_\theta + \frac{2\alpha}{3}\sigma_0\left(\sigma_r + \sigma_\theta\right) = \sigma_0^2, \qquad (4.1.2)$$

$$\begin{aligned}
\dot{\varepsilon}_r^p &= \lambda\left[6\alpha\sigma_0 + 2\left(9 - \alpha^2\right)\sigma_r - \left(2\alpha^2 + 9\right)\sigma_\theta\right], \\
\dot{\varepsilon}_\theta^p &= \lambda\left[6\alpha\sigma_0 + 2\left(9 - \alpha^2\right)\sigma_\theta - \left(2\alpha^2 + 9\right)\sigma_r\right], \qquad (4.1.3) \\
\dot{\varepsilon}_z^p &= \lambda\left[6\alpha\sigma_0 - \left(9 + 2\alpha^2\right)\left(\sigma_r + \sigma_\theta\right)\right],
\end{aligned}$$

$$\varepsilon_r^e = \frac{\sigma_r - \nu\sigma_\theta}{E}, \quad \varepsilon_\theta^e = \frac{\sigma_\theta - \nu\sigma_r}{E}, \quad \varepsilon_z^e = -\frac{\nu\left(\sigma_r + \sigma_\theta\right)}{E}, \qquad (4.1.4)$$

$$\varepsilon_r = \varepsilon_r^e + \varepsilon_r^p, \quad \varepsilon_\theta = \varepsilon_\theta^e + \varepsilon_\theta^p, \quad \varepsilon_z = \varepsilon_z^e + \varepsilon_z^p.$$

(4.1.5)

In addition, the equation of strain compatibility is

$$\rho \frac{\partial \varepsilon_\theta}{\partial \rho} = \varepsilon_r - \varepsilon_\theta \ .$$

(4.1.6)

Eliminating λ in (4.1.3) gives

$$\frac{\dot{\varepsilon}_r^p}{\dot{\varepsilon}_\theta^p} = \frac{\left[6\alpha\sigma_0 + 2\left(9-\alpha^2\right)\sigma_r - \left(2\alpha^2+9\right)\sigma_\theta\right]}{\left[6\alpha\sigma_0 + 2\left(9-\alpha^2\right)\sigma_\theta - \left(2\alpha^2+9\right)\sigma_r\right]},$$

$$\frac{\dot{\varepsilon}_z^p}{\dot{\varepsilon}_\theta^p} = \frac{\left[6\alpha\sigma_0 - \left(9+2\alpha^2\right)\left(\sigma_r+\sigma_\theta\right)\right]}{\left[6\alpha\sigma_0 + 2\left(9-\alpha^2\right)\sigma_\theta - \left(2\alpha^2+9\right)\sigma_r\right]}.$$

(4.1.7)

Equations (4.1.1), (4.1.2), (4.1.4), (4.1.5), (4.1.6), and (4.1.7) can be rewritten as

$$\frac{\partial\sigma_r}{\sigma_0\partial\rho} + \frac{\sigma_r-\sigma_\theta}{\sigma_0\rho} + \frac{\Omega\rho}{\sqrt{3}} = 0,$$

$$\left(1-\frac{\alpha^2}{9}\right)\left(\sigma_r^2+\sigma_\theta^2\right) - \left(1+\frac{2\alpha^2}{9}\right)\sigma_r\sigma_\theta + \frac{2\alpha}{3}\sigma_0\left(\sigma_r+\sigma_\theta\right) - \sigma_0^2 = 0,$$

$$\varepsilon_r^e - \frac{\sigma_r - \nu\sigma_\theta}{E} = 0,$$

$$\varepsilon_\theta^e - \frac{\sigma_\theta - \nu\sigma_r}{E} = 0,$$

$$\varepsilon_z^e + \frac{\nu\left(\sigma_r+\sigma_\theta\right)}{E} = 0,$$

$$\varepsilon_r - \varepsilon_r^e - \varepsilon_r^p = 0,$$

$$\varepsilon_\theta - \varepsilon_\theta^e - \varepsilon_\theta^p = 0,$$

$$\varepsilon_z - \varepsilon_z^e - \varepsilon_z^p = 0,$$

$$\rho\frac{\partial\varepsilon_\theta}{\partial\rho} - \varepsilon_r + \varepsilon_\theta = 0.$$

(4.1.8)

Introduction of the notation leads

$$\frac{\partial \sigma_r}{\sigma_0 \partial \rho} + \frac{\sigma_r - \sigma_\theta}{\sigma_0 \rho} + \frac{\Omega \rho}{\sqrt{3}} = R_1(\rho, \Omega),$$

$$\left(1 - \frac{\alpha^2}{9}\right)\left(\sigma_r^2 + \sigma_\theta^2\right) - \left(1 + \frac{2\alpha^2}{9}\right)\sigma_r \sigma_\theta + \frac{2\alpha}{3}\sigma_0\left(\sigma_r + \sigma_\theta\right) - \sigma_0^2 = R_2(\rho, \Omega),$$

$$\varepsilon_r^e - \frac{\sigma_r - \nu \sigma_\theta}{E} = R_3(\rho, \Omega),$$

$$\varepsilon_\theta^e - \frac{\sigma_\theta - \nu \sigma_r}{E} = R_4(\rho, \Omega),$$

$$\varepsilon_z^e + \frac{\nu\left(\sigma_r + \sigma_\theta\right)}{E} = R_5(\rho, \Omega),$$

$$\varepsilon_r - \varepsilon_r^e - \varepsilon_r^p = R_6(\rho, \Omega),$$

$$\varepsilon_\theta - \varepsilon_\theta^e - \varepsilon_\theta^p = R_7(\rho, \Omega),$$

$$\varepsilon_z - \varepsilon_z^e - \varepsilon_z^p = R_8(\rho, \Omega),$$

$$\rho \frac{\partial \varepsilon_\theta}{\partial \rho} - \varepsilon_r + \varepsilon_\theta = R_9(\rho, \Omega).$$

(4.1.9)

Then, equation (4.1.8) becomes

$$R_i(\rho, \Omega) = 0, \quad 1 \le \mathrm{i} \le 9.$$

(4.1.10)

In order to verify the solution, it is necessary to show that

$$\left|R_i(\rho, \Omega)\right| \le \delta, \quad 1 \le \mathrm{i} \le 9. \qquad (4.1.11)$$

where δ is a small number.

MATHEMATICA provides the solution in terms of interpolating functions. An interpolating function can be differentiated using the command D[]. This command returns another interpolating function. Thus each of $R_i(\rho,\Omega)$ at a given value of $\Omega=\Omega_r$ is a combination of interpolating functions according to (4.1.9) and therefore is an interpolating function. This function can be evaluated at any number of points in the range $a \le \rho \le 1$. As a result, there is a set of value for each of $\left|R_i(\rho,\Omega_r)\right|$. The maximum element of each set can be found using the command Max. Substituting these values into (4.1.11) yields δ .

The above described procedure has been used at

$$\Omega_r = \frac{3\Omega_e + \Omega_p}{4}, \quad \Omega_r = \frac{\Omega_e + \Omega_p}{2}, \quad \Omega_r = \frac{\Omega_e + 3\Omega_p}{4}.$$

As a result, it has been found that $\delta < 10^{-10}$.

5. Conclusions

This article presents a semi-analytic solution for the stresses and strains within a rotating elastic/plastic annular disk. The yield criterion proposed in Drucker and Prager (1952) and its associated flow rule have been adopted. Therefore, in contrast to the solutions presented in Guven (1992), Guven (1998), Orchan and Eraslan (2002), Eraslan and Orcan (2002[a], 2002[b]), Eraslan (2002, 2003), You *et al*. (2000) and Hojjati and Hassani (2008), the equations to be solved involve strain rates rather than strains. This greatly adds to the difficulties of the solution. The method proposed in Lomakin *et al*. (2016) has been used to facilitate numerical analysis. In particular, numerical techniques are only necessary to solve ordinary differential equations and evaluate ordinary integrals. It worthy of note here that the solution depends on two independent variables, Ω and ρ. It is evident from (2.2.11), (2.2.12), (2.2.17), (2.2.22), and (2.2.23) that simple scaling of a single solution for a disk of given geometry, Poisson's ratio and $\alpha-$ value supplies the solutions for similar disks of material with the same Poisson's ratio and $\alpha-$ value but any yield stress and Young's modulus. For example, the numerical solution illustrated in Figures 2 to 9 supplies the solutions for $a=0.3$ disks of material with $\nu=0.3$, values of α shown in the figures but any yield stress and Young's modulus.

For the variable thickness, a new semi-analytic solution for a thin rotating annular disc has been found. A numerical technique is only necessary to solve the ordinary

differential equation (3.1.16). The primary objective of the present paper is to reveal the effect of α involved in the yield criterion (3.1.6) and m involved in Eq. (3.1.3) on the distribution of stress at loading and on the distribution of residual stresses. Note that $\alpha = 0$ corresponds to the von Mises yield criterion and $m = 0$ corresponds to the disc of constant thickness. Therefore, the value of α is a measure of the deviation of the Drucker-Prager yield criterion from the von Mises yield criterion. Based on numerical results obtained the following conclusions can be drawn. The radial stress increases as m increases (Figs. 19 to 22 and the effect of m on the circumferential stress is not so significant as on the radial stress (Figs. 23 to 26). Furthermore, the effect of m on both the radial and circumferential residual stresses is negligible at $\rho_c = 0.3$ (Figs. 27, 28, 31, and 32) and more pronounced at $\rho_c = 0.5$ (Figs. 29, 30, 33, and 34). Finally, the dependence of the circumferential residual stress on m at a given value of ρ is not monotonic (Figs.33 and 34).

Bibliography

Alexandrov, S., 2015. Elastic/Plastic disks under plane stress conditions, Springer, New York, US.

Alexandrov, S., Jeng, Y. R., Lomakin, E., 2011. Effect of pressure-dependency of the yield criterion on the development of plastic zones and the distribution of residual stresses in thin annular disks. J. Appl. Mech.-T ASME 78, 031012.

Alexandrov, S., Jeng, Y.-R., Lomakin, E., 2014. An exact semi-analytic solution for residual stresses and strains within a thin hollow disk of pessure-sensitive material subject to thermal loading. Meccanica 49, 775-794.

Alexandrova, N., 2012. Application of Mises yield criterion to rotating solid disk problem. International Journal of Engineering Science 51, 333-337.

Alexandrova, N., Alexandrov, S., Vila Real, P., 2004. Displacement field and strain distribution in a rotating annular disk. Mechanics Based Design of Structures and Machines 32, 441-457.

Alexandrova, N., Alexandrov, S., 2004. Elastic-Plastic Stress Distribution in a Plastically Anisotropic Rotating Disk. Trans. ASME J. Appl. Mech. 71, 427-429.

Callioglu, H., Topcu, M., Tarakcilar, A.R., 2006. Elastic-plastic stress analysis of an orthotropic rotating disc. Int. J. Mech. Sci. 48, 985-990.

Drucker, D. C., Prager, W., 1952. Soil mechanics and plastic analysis for limit design. Quarterly of Applied Mathematics 10, 157-165.

Eraslan, A. N., 2002. Inelastic deformations of rotating variable thickness solid disks

by Tresca and von Mises criteria. International Journal of Computational Engineering Science 3, 89-101.

Eraslan, A. N., 2003. Elastoplastic deformations of rotating parabolic solid disks using Tresca's yield criterion. European Journal of Mechanics A/Solids 22, 861-874.

Eraslan, A. N., Orcan, Y., 2002[a]. Elastic-plastic deformation of a rotating solid disk of exponentially varying thickness. Mechanics of Materials 34, 423-432.

Eraslan, A. N., Orcan, Y., 2002[b]. On the rotating elastic-plastic solid disks of variable thickness having concave profiles. International Journal of Mechanical Sciences 44, 1445-1466.

Guven, U., 1992. Elastic-plastic stresses in a rotating annular disk of variable thickness and variable density. International Journal of Mechanical Sciences 34, 133-138.

Guven, U., 1998. Elastic-plastic stress distribution in a rotating hyperbolic disk with rigid inclusion. International Journal of Mechanical Sciences 40, 97-109.

Hojjati, M. H., Hassani, A., 2008. Theoretical and numerical analyses of rotating disks of non-uniform thickness and density. International Journal of Pressure Vessels and Piping 85, 694-700.

Jeong, W., Chung, K., 2016. Stress analysis of rotating annular hyperbolic disks obeying a pressure-dependent yield criterion. Structural Engineering and Mechanics 58, 689-705.

Kao, A. S., Kuhn, H. A., Spitzig, W. A. Richmond, O., 1990. Influence of superimposed hydrostatic pressure on bending fracture and formability of a low carbon steel containing globular sulfides. Trans. ASME J. Eng. Mater. Technol. 112, 26-30.

Liu, P. S., 2006. Mechanical behaviors of porous metals under biaxial tensile loads. Materials Science and EngineeringA422, 176-183.

Lomakin, E., Alexandrov, S., Jeng, Y.-R. , 2016. Stress and strain fields in rotating elastic/plastic annular disks. Archive of Applied Mechanics 86, 235-244.

Orcan, Y., Eraslan, A. N., 2002. Elastic-plastic stresses in linearly hardening rotating solid disks of variable thickness. Mechanics Research Communications 29, 269-281.

Pirumov, A., Alexandrov, S., Jeng, Y.-R., 2013. Enlargement of a circular hole in a disk of plastically compressible material. Acta Mechanica 224, 2965-2976.

Rees, D.W.A., 1999. Elastic-plastic stresses in rotating disks by von Mises and Tresca. ZAMM 19, 281-288.

Spitzig, W. A., Sober, R. J., Richmond, O., 1976. The effect of hydrostatic pressure on the deformation behavior of maraging and HY-80 steels and its implications for plasticity theory. Metallurg. Trans. 7A, 1703-1710.

Timoshenko, S. P., Goodier, J. N., 1970. Theory of Elasticity 3rd ed., McGraw-Hill, New York, US.

Wilson, C. D., 2002. A critical reexamination of classical metal plasticity. Journal of Applied Mechanics Transactions ASME 69, 63-68.

You, L. H., Tang, Y. Y., Zhang, J. J., Zheng, C. Y., 2000. Numerical analysis of elastic-plastic rotating disks with arbitrary variable thickness and density. International Journal of Solids and Structures 37, 7809-7820.

초 록

본 논문에서는 압력 의존적 항복 기준을 만족하는 회전 환상 원판의 응력과 변형율을 분석하였다. 드러커-프레이저 항복 기준은 평면 응력 조건하의 회전 환상 원판내의 탄성/소성 응력과 변형율을 구하기 위해 연관 흐름 이론과 연결되어 사용된다. 회전 원판의 분선을 위해 사용된 기존의 이론들과 비교했을 때 본 모델의 주요한 특징은 물질이 소성적으로 압축된다는 점이다. 또한, 다른 모델들과 대조적으로 구성 방정식이 변형율이 아니라 변형속도와 관련된다. 그러나, 제안된 방법을 적용하면 변형속도에 대한 해는 한 개의 비선형 상미분 방정식과 두 개의 선형 상미분 방정식으로 귀결된다. 이 방정식들은 하나씩 차례로 풀 수 있는 데, 이 과정은 수치 처리를 간략히 하고 수치해의 정확도를 높여준다. 변형율 해를 구하기 위해서는 상적분을 위한 수치방법이 요구된다. 일반해를 구하기 위해 한 예가 제시되었다. 이 논문의 주요 목적은 드러커-프레이저 항복기준이 폰-미즈지 항복기준으로부터 벗어난 정도를 조절하는 인자효과와 응력과 잔류응력의 분포에 영향을 미치는 쌍곡선형을 통제하는 기하인자효과를 연구하는 것이다.

주요어: 회전 환상 원판, 소성 항복, 드러커−프레이저 항복 기준

학 번: 2012-30919